BNL-101913-2014-TECH
AD/RHIC/1;BNL-101913-2013-IR

Scenario for the Relativistic Heavy Ion Collider (RHIC) for Brookhaven National Laboratory

A. G. Ruggiero

May 1984

Collider Accelerator Department
Brookhaven National Laboratory

U.S. Department of Energy
USDOE Office of Science (SC)

DISCLAIMER

High Energy Facilities
Advanced Projects
BROOKHAVEN NATIONAL LABORATORY
Associated Universities, Inc.
Upton, New York 11973

RHIC Technical Note No. 1

SCENARIO FOR THE RELATIVISTIC HEAVY ION COLLIDER (RHIC) FOR BROOKHAVEN NATIONAL LABORATORY

A. G. Ruggiero

May 1984

BNL-35127
INFORMAL REPORT

HIGH ENERGY FACILITIES
Advanced Projects

SCENARIO FOR THE RELATIVISTIC HEAVY ION COLLIDER (RHIC) FOR BROOKHAVEN NATIONAL LABORATORY

A. G. Ruggiero

May 1984

B R O O K H A V E N N A T I O N A L L A B O R A T O R Y
A S S O C I A T E D U N I V E R S I T I E S, I N C.
UPTON, LONG ISLAND, NEW YORK 11973

Under Contract No. DE-AC02-76CH00016
UNITED STATES DEPARTMENT OF ENERGY

Preface

This paper has been used three times as reference material for three technical review committees (Willis Committee, April 1-3 and April 30-May 1; Bromley Committee, May 3-4, 1984). It has also been the baseline from which most of the Design Report on RHIC has been derived.

This document summarizes the work and contribution of several people during the period November 1, 1983, when the RHIC Task Force was formed, and May 1984 when the compiler of this work left the Task Force to return to his original institution (Fermilab).

The list of people involved would be quite too long if one wants to give credit even to the smallest but sometime essential contribution. It is made of very talented and skilful professionals in the field of accelerator physics. Nevertheless it is mandatory that the compiler expresses his gratitude and appreciation very explicitly to J. Claus, H. Hahn, G. Parzen and G. Young (ORNL). Without the intensity and hardship of the work of these people, the RHIC project as it stands today could have not been made possible.

Table of Contents

SUMMARY

In this note we describe a scheme to obtain a high performance relativistic heavy ion collider (RHIC) sized to fit within the CBA tunnel at BNL.

The project has two parts: the Source of heavy ions and the Collider itself. We keep these two parts separated since a different analysis is to be done for each. It is obvious that the performance of the total facility depends crucially on the performance of both.

The layout of the whole project (Source and Collider) is shown in Fig. 1.

THE SOURCE

The Source has the following parts:

1. The negative-ion source
2. The Tandem van de Graaff
3. The Booster Ring
4. The AGS

A proposed new addition to the BNL facilities is the Booster Ring. Also included are transfer lines from the Tandem to the Booster, and from the Booster to the AGS. Figure 2 gives a more detailed map of the Source layout.

1. The Negative-Ion Source

The nuclear species proposed for colliding beam experiments are given in Table 1. These are adequate to cover most of the experimental program with the Collider since their atomic mass varies as n^3 with n an integer. They have also been chosen because they can easily be produced as negative-ions to be fed into the source for the Tandem.

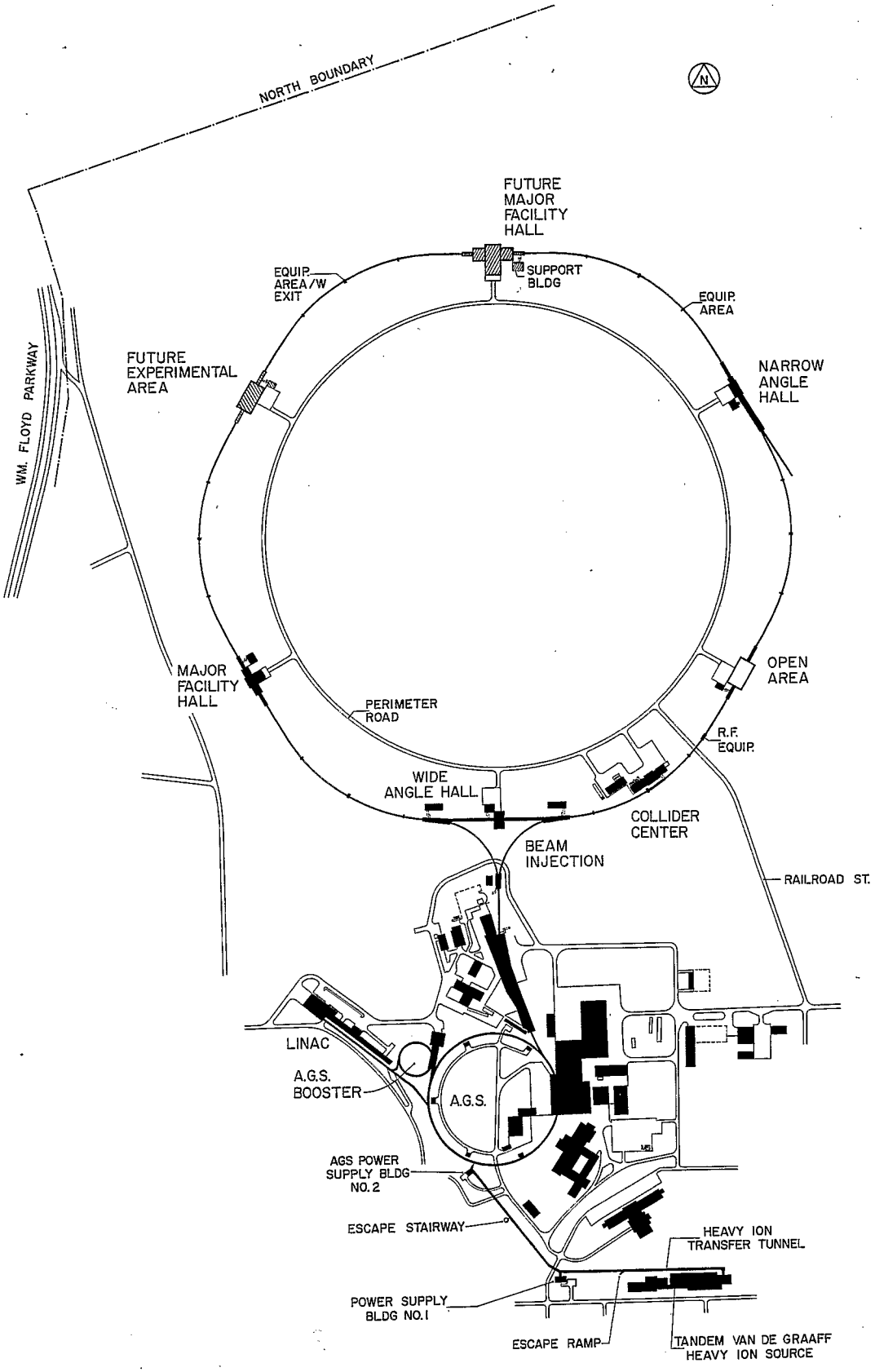

Fig. 1. Layout of RHIC project - collider and source

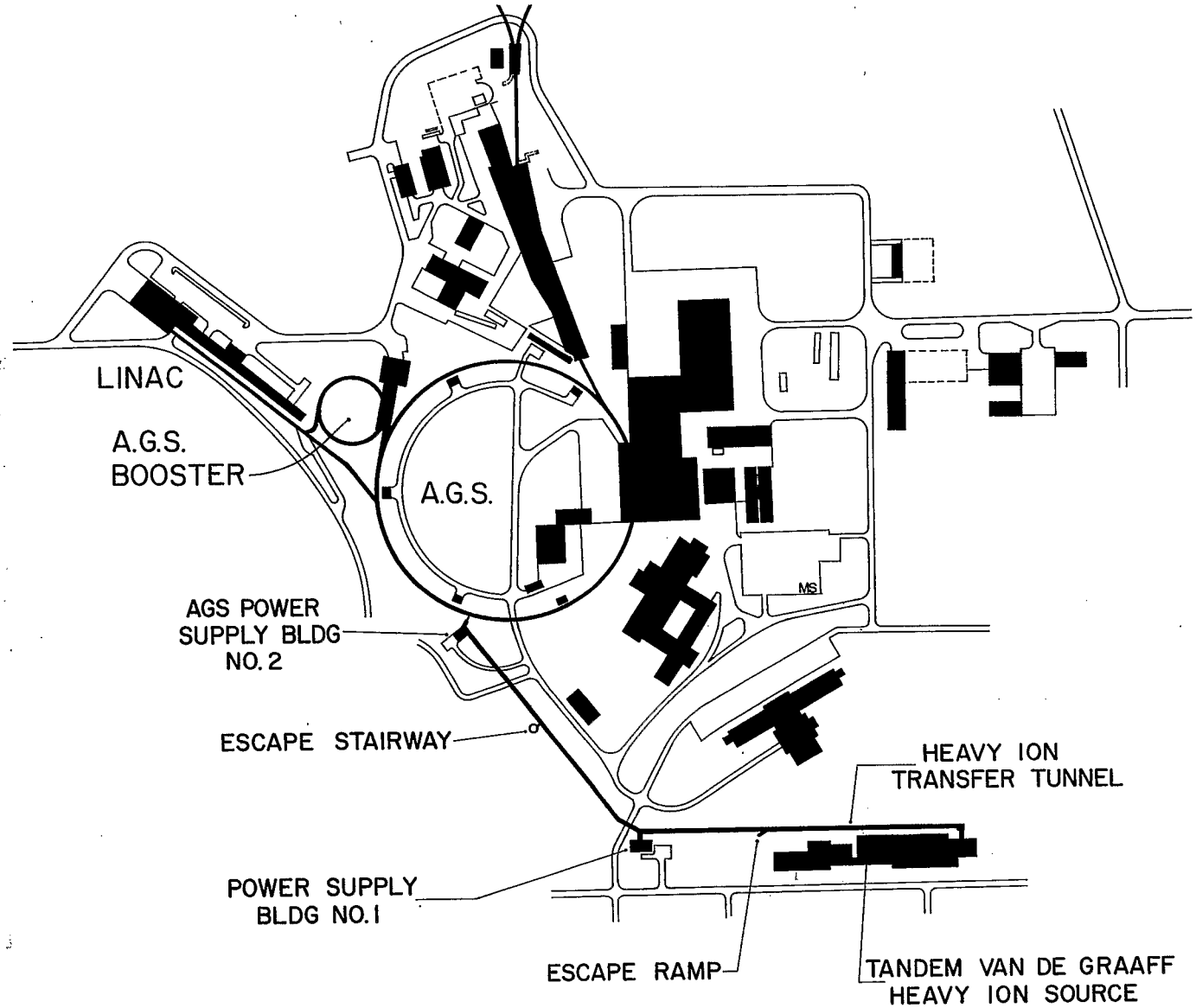

Fig. 2. Injection system for collider

Table 1. Proposed Ion Species for RHIC

Deuterium	(n)	Atomic No. Z	Mass No. A	Rest Energy GeV/A	A/Z
Proton	(1)	1	1	0.9383	1.0
Deuterium	(1)	1	2	0.9375	2.0
Carbon	(2)	6	12	0.9310	2.0
Sulphur	(3)	16	32	0.9302	2.0
Copper	(4)	29	63	0.9299	2.2
Iodine	(5)	53	127	0.9302	2.4
Gold	(6)	79	197	0.9308	2.5

Typical currents which can be generated at the source for these elements are around 200 micro-amp-particle, except for deuterium for which we can expect as much as one milli-amp-particle. Of course protons are generated by a different and higher intensity source: the 200 MeV Linac.

2. The Tandem van de Graaff

We propose two-stage operation of the Tandem. The three-stage mode has also been examined. It would require the addition of the -9 MV (negative) potential terminal. Although in this mode higher energies and intensities are possible, the operation is nevertheless more unreliable and difficult since it requires manipulating the negative-ion source at high-negative potential. With the two stage mode of operation the source is at ground potential and therefore easy to reach and to operate.

In the first stage, (see Fig. 3), the negative ions (Q = -1) are accelerated from ground to a +15 MV potential. At this point the kinetic energy of the negative ions is 15 MeV, and in the high-voltage terminal they hit the first stripping target. The most probable charge state Q_T which results depends

on the element as shown in Table 2. The ions are next accelerated by the second stage, increasing their energy by (+15 MV)Q_T. In Table 2 we give also the most probable charge state Q_F of the ions after the second stripping target, which is located at the end of the Tandem. Of course there is no need for the second target in the case of the deuterium beam, since it would be completely stripped by the first target.

The expected stripping efficiencies S_T and S_F are also given in Table 2. The Tandem output currents are calculated by taking into account the stripping efficiencies and an overall Tandem transmission efficiency of 75%. The following cycle is proposed: the pulse length is at most 100 micro-sec long, and the repetition period is 1.2 sec to match the Booster Ring and the AGS cycles.

There is good experimental evidence that suggests the beam quality (intensity, emittance and energy spread) remains constant over the length of the pulse. More experimmental work is planned to corroborate this fact for any element chosen. In the meantime we assume this for the purpose of our design.

Table 2. Tandem Operation Parameters*

Element	Q_T	S_T	Kinetic Energy MeV/A	β_F	Q_F	S_F	Current μ-amp-part
Deuterium	+1	70%	15.0	.1768	+1	100%	525.
Carbon	+5	61	7.5	.1262	+6	90	82.
Sulphur	+9	34	4.7	.1002	+14	40	20.
Copper	+11	27	2.9	.0782	+22	27	11.
Iodine	+13	20	1.65	.0595	+31	20	6.
Gold	+13	19	1.0	.0463	+36	17	5.

*Two-Stage Mode - 75% transmission efficiency.

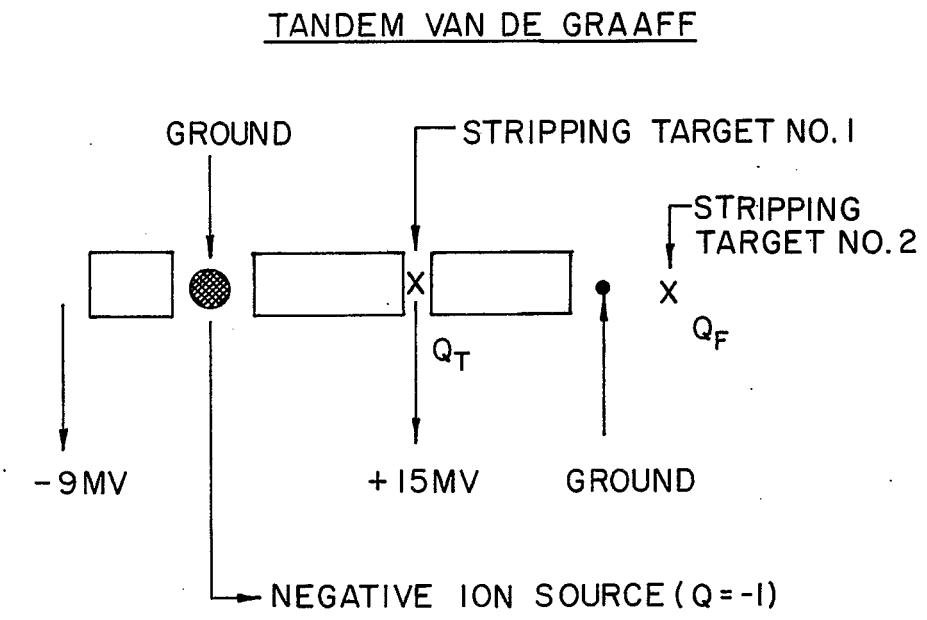

Fig. 3. Tandem van de Graaff with stripping targets

At the end of the Tandem, just prior to the last stage of stripping, the total beam emittance should not exceed 1 π mm-mrad, and the relative kinetic energy spread is around 10^{-4}, mostly due to power supply regulation errors. Again we assume that this applies for any element chosen. The beam, once injected into the Booster, is captured by the single (h = 1) rf bucket which covers the entire circumference of the Booster, and thus does not need to be prebunched.

The stripping target at the end of the Tandem would be made of a carbon foil, 20 $\mu g/cm^2$ thick for gold and thinner for lighter ions. For gold, which is the extreme case, we expect an rms scattering angle of 1.9 mrad when traversing the foil. To minimize the effect on the beam emittance growth, it is important to locate the stripper foil in a place in the transport line following the Tandem where the lattice function β does not exceed 30 cm in either plane. The associated emittance growth is then no more than 1 π mm-mrad and the total value should not exceed 2 π mm-mrad for any of the species taken into consideration.

When traversing the stripping target, ions also experience an energy loss. The largest figure, for gold, is about 10.5 keV/A. An energy spread is also introduced with an rms value typically one-tenth of the energy loss. Although the energy loss is not significant, the spread in energy is rather important. For gold it amounts to a momentum spread (at injection into the Booster) of $\Delta p/p = \pm 0.11\%$. The longitudinal area for this debunched beam coasting into the Booster is then 0.065 eV•sec/A. For lighter ions these values are smaller.

The details of the transfer line between the Tandem and the Booster (through the AGS) are given in Fig. 4.

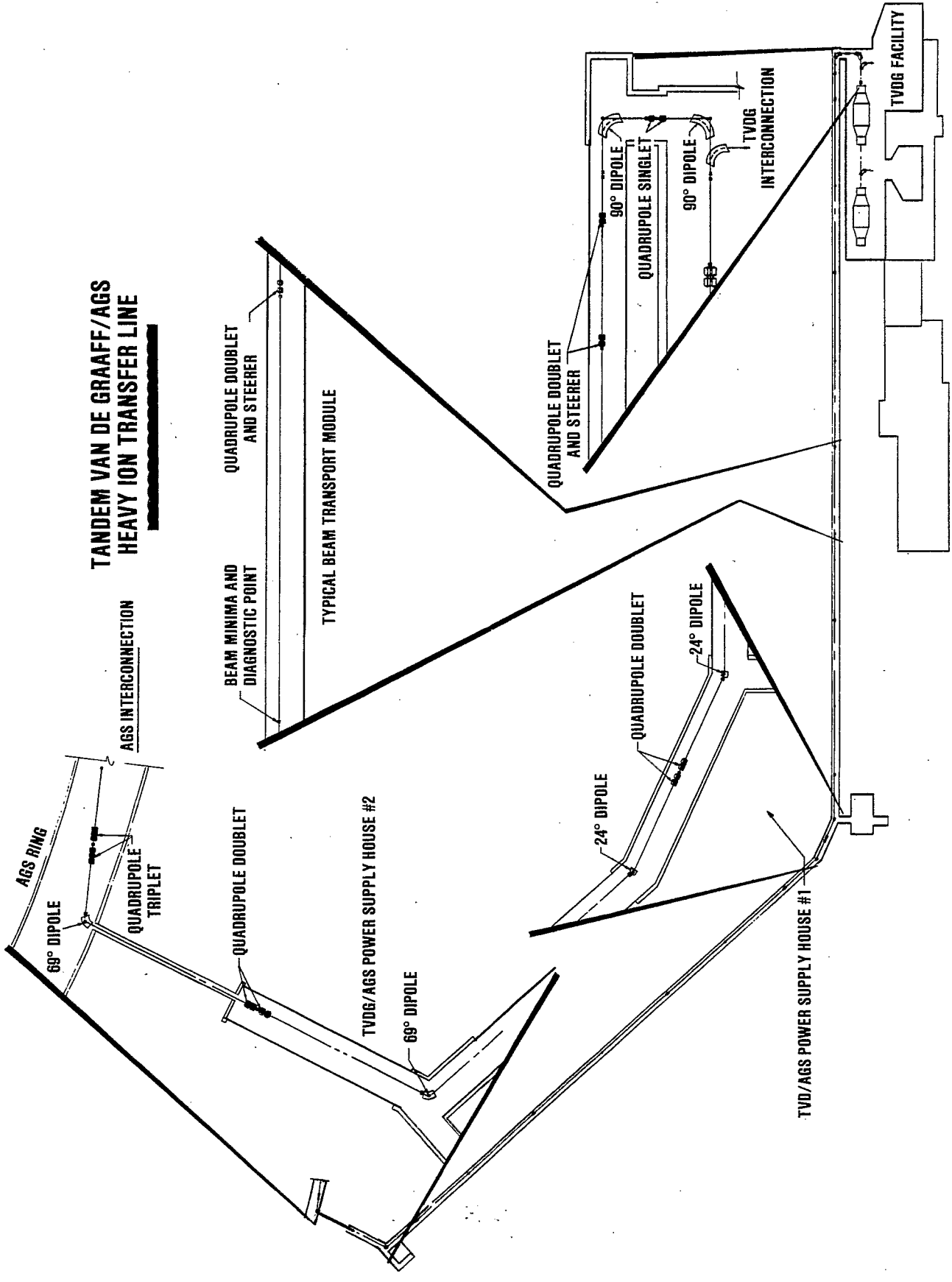

Fig. 4. The transport line between the tandem and the booster

We have also considered the possibility of adding, at the end of the Tandem, a section of a so-called Heidelberg Linac. This would considerably enhance the beam energy from 1 to perhaps 5 MeV/A for gold, and the beam velocity would also double, from $\beta = 0.0463$ to $\beta = 0.1$. There are two positive effects with this addition. First, because of the higher energy, the space charge limitation in the Booster is softened and more particles can be injected, provided the Tandem is capable of providing a longer pulse ($\sim$150 μsec) and/or more intensity. Second, the ions can be stripped to a higher charge state before being injected into the Booster, and this fact, for the Booster's fixed maximum magnetic rigidity, would allow larger output energies. This is important for gold since it would also increase the efficiency in the last stripping target (between Booster and AGS). Unfortunately the gain in intensity is modest, only a factor of two, and this gain is cancelled when a 50% efficiency for 100 MHz bunching to accelerate the beam through the Linac is taken into account. We have not included this piece of equipment in our scenario since we do not foresee any significant improvement with it for the Collider Project itself.

3. The Booster Ring

The circumference of this ring is just one quarter of the AGS circumference. The most important parameters are listed in Table 3. A plan view of the ring is given in Fig. 5. A plot of the lattice functions is shown in Fig. 6.

We assume that the betatron acceptance is 50 π mm-mrad in both planes. It could be larger in the horizontal plane, but very likely the extra amount is not useful because of possible linear and non linear coupling between the two modes of oscillations which cannot be avoided.

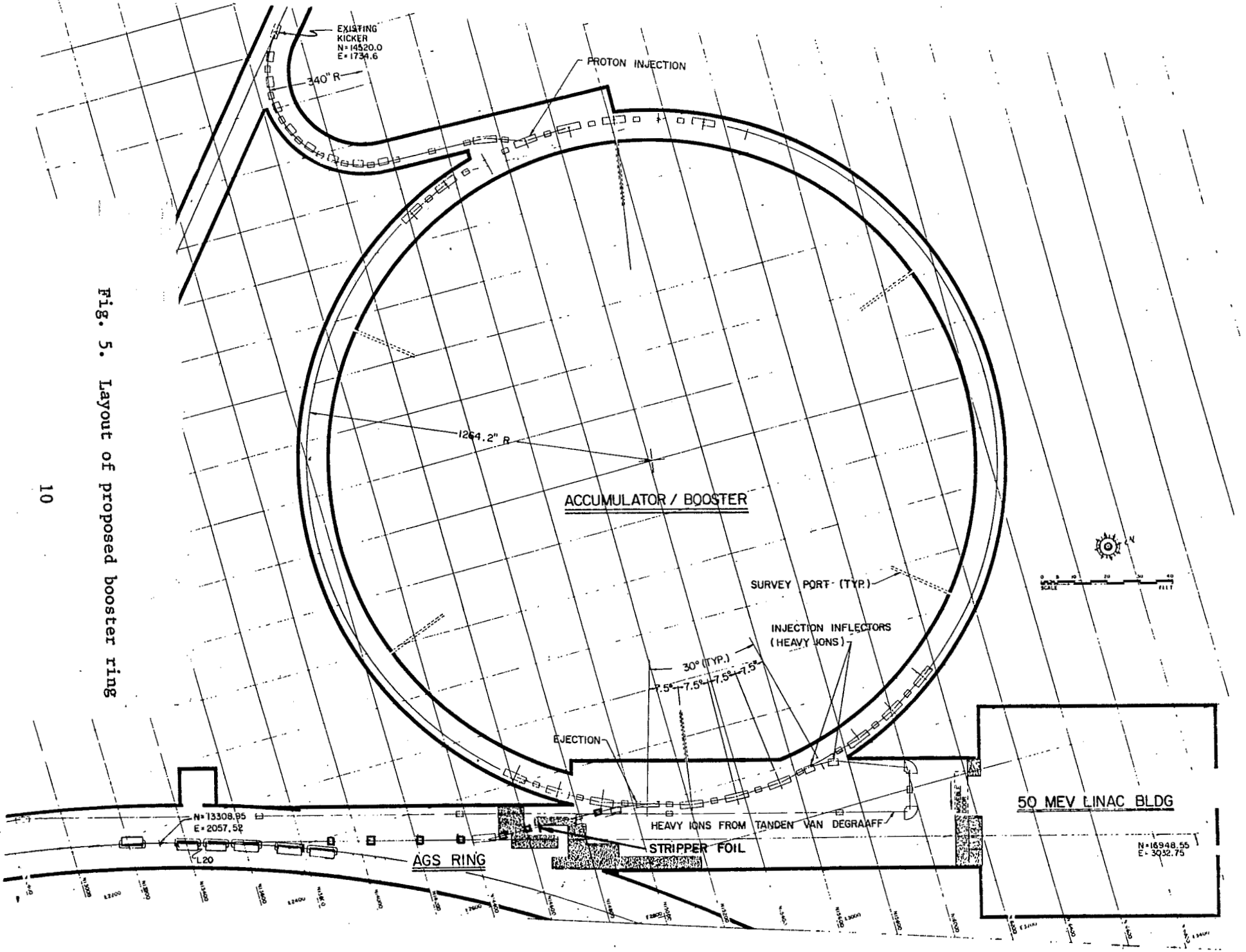

Fig. 5. Layout of proposed booster ring

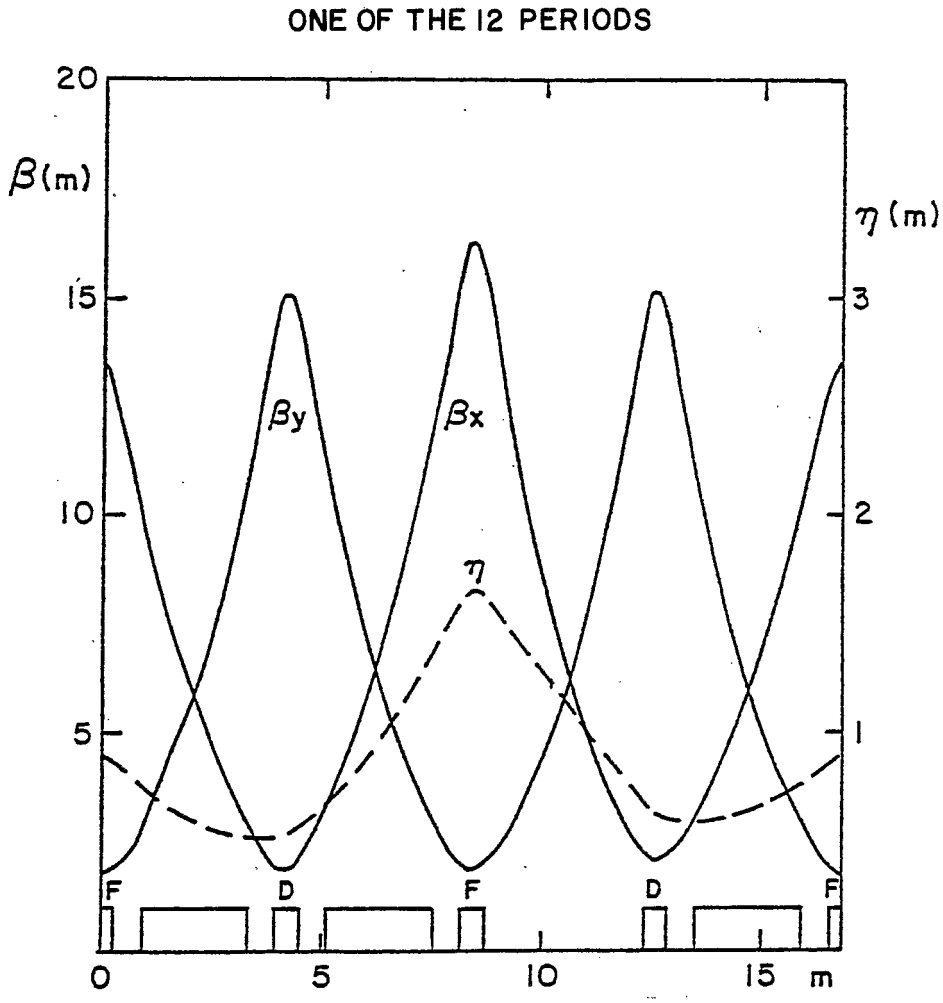

Fig. 6. Amplitude and dispersion of functions for booster ring lattice

Table 3. Booster Ring Parameters

Circumference		201.84 m
Periodicity		12
Period Structure:	QF/2 O B O QD/2 QD/2 O B O QF/2 QF/2 S QD/2 QD/2 O B O QF/2	
Drifts:	O	0.5516 m
	S	3.703 m
Phase Advance/Cell		100.5°
Betatron Tunes, H and V		~6.7
Transition Energy, γ_T		6.5
β_{max}/β_{min}		16m/2m
η_{max}		1.7 m
Dipole (B):	Length	2.4 m
	Max. Field	12 KG
	Bending Radius	13.751 m
	Aperture, HxV (full)	3.25 x 10 in^2
Quads (QF/2,QD/2):	Half-Length	0.25 m
	Bore Radius	4 in.
	Max. Pole Tip Field	12.7 KG

The beam is injected into the Booster and stacked in the betatron phase space by filling the machine circumference with the beam pulse for some number, n, of consecutive turns which corresponds to a total number of particles N_B. It is assumed that the beam will quickly fill up the available acceptance in both planes, with the help eventually of other available steering means, until the space charge limit is reached. This corresponds to a maximum number N_{SC} of particles that can be injected according to the formula

$$\frac{N_{SC}}{\varepsilon_N} = (\beta\gamma^2)\,\frac{4\pi B_f \Delta\nu}{3 r_o F}\,\frac{A}{Q_F^2}\,. \qquad (1)$$

B_f is the bunching factor, defined as the ratio of the average current to the peak current, $\Delta\nu$ is the maximum allowable tune shift, A the mass number, Q_F the charge state, $r_o = 1.535 \times 10^{-18}$ m, and F a form factor that for $\beta << 1$ is very close to 1. On the left-hand side of equation (1), ε_N is the normalized emittance; the actual emittance is given by

$$\varepsilon = \varepsilon_N/(\beta\gamma). \qquad (2)$$

Here the emittances are as usual always given in πmm-mrad units. It is important that the phase space density, N_B/ε_N, is as large as possible since the luminosity in the collider depends on this quantity, provided that no other effect causes even a stronger limitation than the space charge at injection. The luminosity also depends upon N_B itself. It is therefore essential to get the largest density, N_B/ε_N, and the largest number, N_B, of particles in the Booster. An important side effect is that, by increasing N_B, one also increases the number of particles that can be transferred to the Collider per AGS pulse and this reduces the Collider filling time.

There is some uncertainty in the value to assign to B_f and $\Delta\nu$. We propose here a bunching factor of 0.5 and $\Delta\nu = 0.1$. The bunching factor of 0.5 corresponds to the rf capture process at injection and to the early stage of acceleration in the Booster. As the beam velocity increases during acceleration the bunching factor can be lowered correspondingly.

The different species are injected into the Booster with no further stripping; that is, with the charge state Q_F as shown in Table 2. Table 4 gives the maximum number N_{SC} of particles that can be injected with the corresponding normalized emittance ε_N. In Table 4, we also give the revolution period T_{rev} and the number N_B of particles with n=8 turns injected, assuming the beam

Table 4. Beam Intensity, Emittance at Injection into the Booster

Element	ε_N π•mm•mrad	T_{rev} μsec	N_B* x 10^9	$N_{S.C_9}$ x 10^9
Deuterium	8.8	3.81	100.	438.
Carbon	6.3	5.33	22.	37.
Sulphur	6.0	6.72	6.7	11.
Copper	3.9	8.60	4.7	5.5
Iodine	3.0	11.31	3.4	3.2
Gold	2.3	14.53	3.6	2.2

*With 8-turn injection

current values given in Table 2. The largest number of turns that can be efficiently injected in one plane is taken here to be 8, and this corresponds to a dilution factor as large as 6.25. By inspecting Table 4 one can see that the beam intensity is limited by the Tandem currents for the lighter ions up to copper. For copper the Tandem current output is about the space charge limit at injection into the Booster. For iodine and gold very clearly there is a space charge limitation by a factor as large as 2. The particle numbers in the dashed squares are those proposed for the estimates in our scheme. For gold only 4 or 5 turns are required to be injected.

The beam is captured at injection by a rf system of harmonic number h=1, so that only one bunch is used and all the particles given in Table 4 are in this bunch. As we have seen, the longitudinal beam area can be as large as 0.065 eV•sec/A for gold at injection. An rf voltage of 0.5 kV makes a bucket area of 0.2 eV•sec/A, also for gold. The rf bucket will be standing-by and the

beam will be made to bunch by diluting itself into this bucket until it is completely full. To avoid further dilution this bucket area is preserved as much as possible during the early stage of the acceleration cycle. The acceleration period is taken to be 0.6 sec for gold and the overall repetition rate 0.8 Hz. In the middle of the cycle a maximum voltage of 30 kV is required. Toward the end of the acceleration, the bunch is made short enough to match the length of the rf buckets in the AGS. The expected rms bunch length at ejection is as small as 20 nsec.

Assuming a top field of 12 KG, we have a maximum kinetic energy of 367 MeV/A for gold which corresponds to $\beta\gamma = 0.971$. To minimize the amount of rf frequency swing it is sufficient to accelerate the lighter ions to the same value which corresponds to the full acceleration for gold. In this case the required frequency swing covers the range of β-values from 0.046 to 0.7. Observe that the ion beam will never have to cross the Booster transition energy during its acceleration.

A vacuum of 10^{-10} mmHg seems to be quite adequate for the survival of practically all the beam against electron capture or loss processes during the acceleration cycle. The beam losses would be about 2%.

After extraction from the Booster and on their way to the AGS the ions pass through one more stripping target. The ions injected into the AGS are then completely stripped. We expect a 50% beam loss for gold, 20% for iodine and 5% for copper and sulphur. Carbon and deuterium do not need further stripping. The last stripping is accomplished with a foil of copper that, for gold, is 70 mg/cm^2 thick. The rms scattering angle associated with this target is 0.7 mrad for gold. If one does not allow more than 1 πmm-mrad increases

in emittance, the stripper foil must be installed in a location where the lattice function β does not exceed 2 meters in both planes.

The energy loss associated with this target is 5 MeV/A and the resulting energy spread (rms) is 0.5 MeV/A. To minimize the increase of the bunch longitudinal area, it is important that the beam is as tightly bunched as possible when crossing the target. For instance, provided that the beam has preserved its original bunch area of 0.2 eV•sec/A, an rms bunch length of 20 nsec would give an energy spread in the beam also of 0.5 MeV/A (rms), which is comparable to the spread introduced by hitting the target. It seems that an appreciable increase in the bunch area cannot be avoided.

4. The AGS

The major parameters of the ring are given in Table 5. Since the injection energy is 367 MeV/A and the ions are completely stripped, there is no requirement for improvement in either the vacuum or the rf system. The accelerator is well suited for the acceleration of the ions to the maximum energy. With the present vacuum of 10^{-7} torr the beam losses are mostly from the electron capture process and would be less than 3%.

Our scenario is the transfer of one bunch at a time from the Booster to the AGS; acceleration to the top energy and then transfer to the Collider. The AGS cycle rate is taken to be 0.8 Hz, and it is assumed that about one minute is needed for the acceleration. The transfer line between the booster and the AGS is shown in Fig. 7.

Taking into account the increase in the beam emittance due to the final stripping, and with $\beta\gamma = 0.971$, at transfer, the emittance values given in Table 4 are just about those the beam would have when injected into the AGS. These emittances are considerably smaller than the ring betatron acceptance.

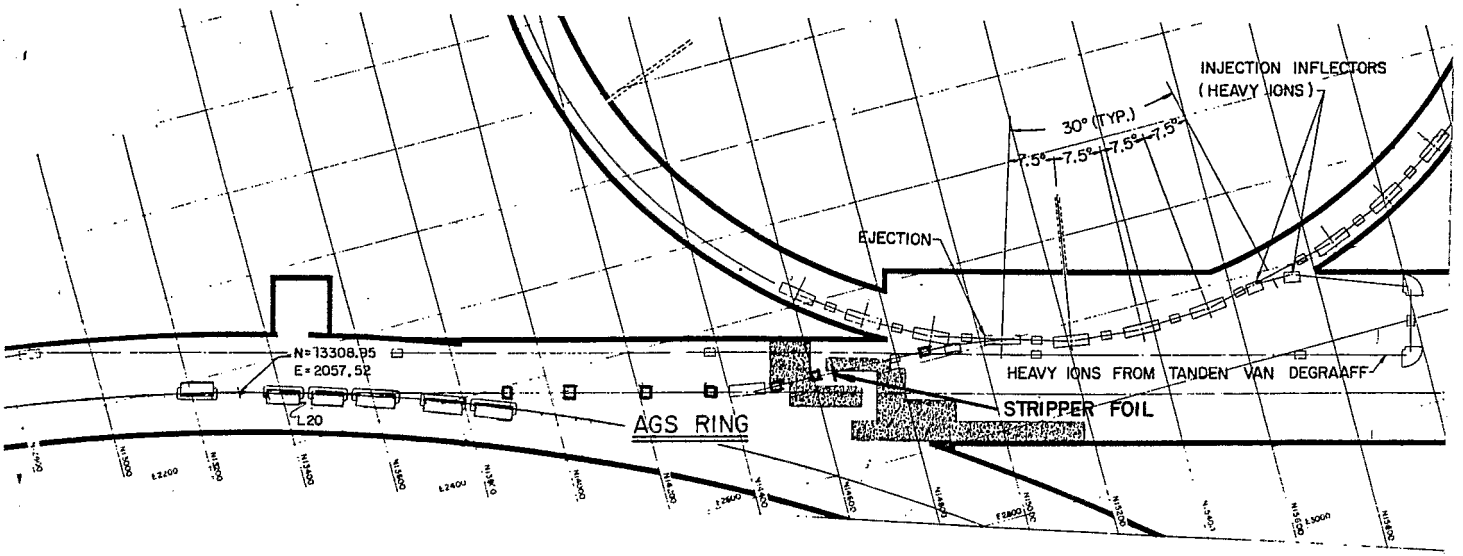

Fig. 7. Transport line between the booster and the AGS

Table 5. AGS Parameters

Circumference	807.11 m
Periodicity	12
Betatron Tunes, H and V	$\sim$8.7
Transition Energy, γ_T	8.5
Betatron Acceptance	$\sim$30 πmm•mrad
Injection Energy (proton)	200 MeV
Ejection Energy (proton)	28 GeV
RF Frequency	2.5-4.457 MHz
Harmonic Nubmer, h	12
Peak RF Voltage	300 KV
Magnetic Rigidity, Bρ at extraction	96.5 KG-m

There is some uncertainty in the value to assign to the beam longitudinal emittance. The values which correspond to injection into the Booster are small, but we expect some dilution during the capture process and the acceleration cycle. A realistic estimate is 0.3 eV•sec/A, including the energy spread from hitting the last stripping target, and we use this figure as input to the design of the Collider. On the other hand, the rf buckets in the AGS are the smallest at injection. If we assume a constant voltage of 300 kV, the bucket area is not less than 1.0 eV•sec/A. At the end of the acceleration in the AGS, the ion bunch is tailored so that it will fit within one of the rf buckets in the Collider. For this purpose we take a final total bunch length of 17 nanosec.

THE COLLIDER

The transfer lines connecting the AGS to the two magnetic rings are part of the Collider system. Their design is the same as in the latest CBA/ISABELLE proposal. A layout of the transport lines is shown in Fig. 8. The two rings and transfer lines will be accommodated in the CBA tunnels which exist on site.

Each ion bunch accelerated in the AGS is extracted and transferred to one of the two Collider Rings. The bunch is captured by a stationary rf bucket. It is essential that the shape of the bunch prior to extraction from the AGS is tailored to match the shape of the buckets in the Collider. Major parameters of the Collider Rings are given in Table 6.

Beam parameters at injection are given in Table 7. It is assumed that, because of the required manipulations, the betatron emittances and the longitudinal phase space area are somewhat diluted to the final values shown in Table 7. We take them to be the same for all species, except protons, which have a larger emittance and a considerably larger number of particles.

The bunch area, S, and the beam emittance, ε, are defined for 95% of the beam population by

$$S = 6 \pi \sigma_\tau \sigma_E \ , \tag{3}$$

where σ_τ is the rms bunch length in unit of time and σ_E the rms energy spread.

$$\varepsilon = 6\pi \frac{\sigma^2_{H,V}}{\beta_{H,V}} \ , \tag{4}$$

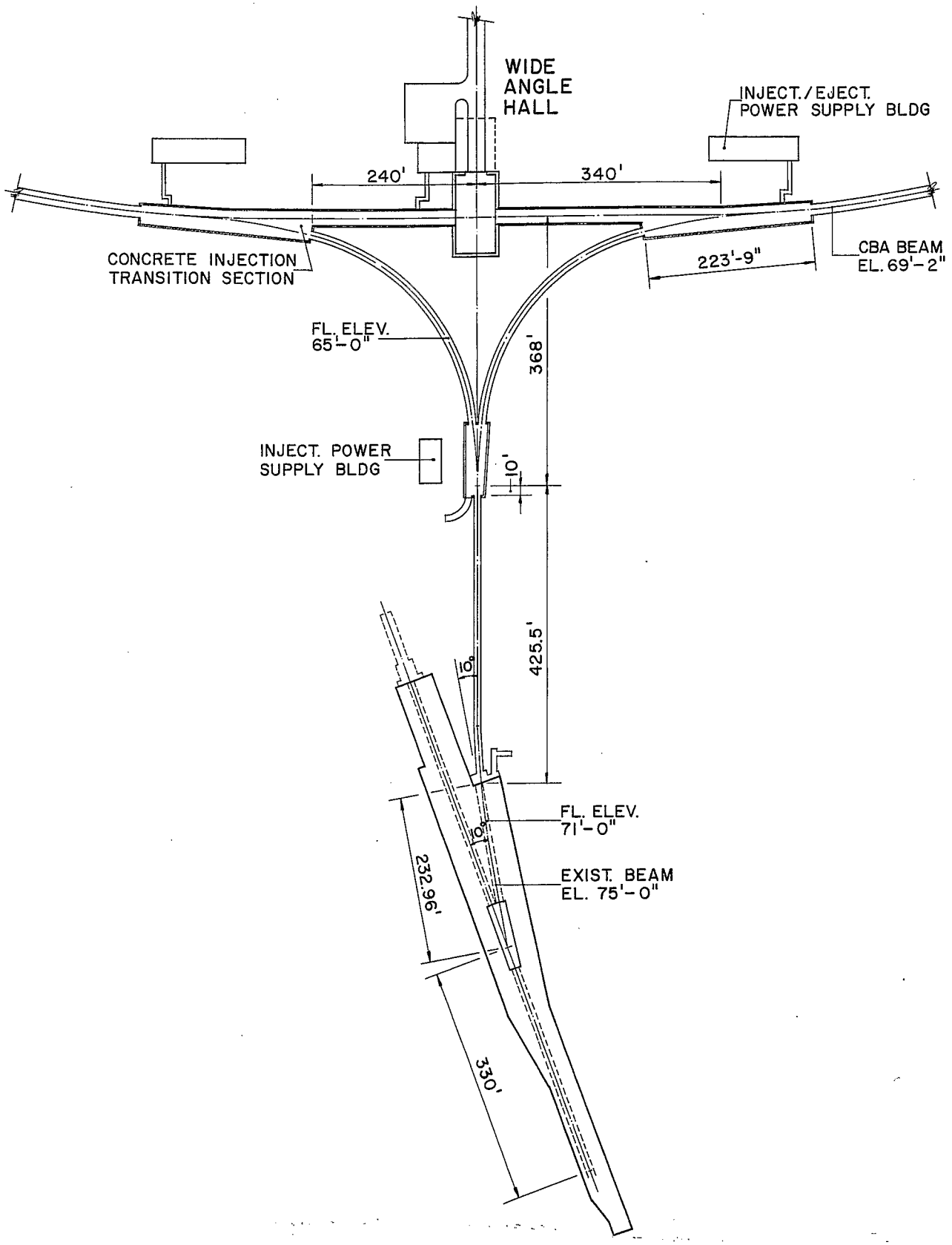

Fig. 8. Accelerator injection plan

Table 6. General Parameters for the Collider

Circumference	3833.8 m
Revolution Frequency ($\beta = 1$)	78.1972 KHZ
Filling Mode	Box - Car
No. of Bunches/Ring	57
Filling Time/Ring	$\sim$ 1 minute
Perodicity	3 (6)
Magnetic Rigidity, B_p:	
at injection	9.65 T-m
at top energy	839.5 T-m
Transition Energy, γ_T	26.4
Natural Chromaticity, H,V	-73.5/-64.8
Betatron Tunes, $\nu_{H,V}$	34.4

Table 7. General Beam Parameters for the Collider

Element	Proton	Deuterium	Carbon	Sulphur	Copper	Iodine	Gold
Injection: Kinetic Energy, GeV/A	28.	13.6	13.6	13.6	12.4	11.2	10.7
β	.99947	.99947	.99793	.99794	.99757	.99704	.99680
Norm. Emitt., ε_N πmm•mrad	20	10	10	10	10	10	10
Bunch Area, S eV•sec/A	0.3	0.3	0.3	0.3	0.3	0.3	0.3
Bunch Length, nsec	$\pm$ 8.6	$\pm$ 8.6	$\pm$ 8.6	$\pm$ 8.6	$\pm$ 8.6	$\pm$ 8.6	$\pm$ 8.6
Energy Spread, $\pm 10^{-4}$	3.8	7.6	7.6	7.6	8.3	9.2	9.6
No ions/Bunch, x10^9	1000	100	22	6.4	4.5	2.6	1.1
Top Energy: Kinetic Energy, GeV/A	250.7	124.9	124.9	124.9	114.9	104.1	100.0
$\beta\gamma$	268.2	134.2	135.2	135.3	124.6	112.9	108.4

where $\sigma_{H,V}$ is the rms beam width or height and $\beta_{H,V}$ the horizontal or vertical amplitude lattice functions. The relation between the actual emittance and the normalized emittance is given by eq. (2).

The bunch dimensions are for 95% of the beam. The bunch length given is the smallest one can obtain from the AGS with present unmodified rf system.

The number of ions per bunch transferred to the Collider is also given in Table 7. It was derived from Table 4 after adjusting for the losses between the Booster and the AGS. Assuming a maximum rigidity of 839.5 T-m we give, also in Table 7, the maximum kinetic energy that can be reached in the Collider Rings.

The two rings are filled in box-car fashion. The total number of bunches accepted is 57 per ring; an equivalent number of AGS pulses is required which gives a filling time of a little more than one minute per ring. The situation is different for the proton beam since 12 bunches can be accelerated simultaneously in the AGS; thus only five AGS pulses would be required and the filling time is less than ten seconds.

The choice of 57 bunches is a direct consequence of the fact that the Collider circumference is 4.75 times the AGS circumference and that there are 12 bunches (at least for protons), equally spaced, transferred from the AGS to the Collider. In the box-car filling mode the transfer is bunch-to-bucket and therefore the rf frequency must have an harmonic number equal to an integer times 57. The largest integer is 12 since it corresponds to a bucket length which is just about the length of the injected bunches.

The bunch separation is 67 meters and this corresponds to a rise/fall time of 200 nano-sec for the injection kickers.

1. The Lattice. The Arcs.

The two Collider rings are identical. They are placed in the CBA tunnel side by side. The separation is 30 cm between the beam axes. The geometry of the two rings is such that the arcs and the straight sections follow very closely the center of the CBA tunnel.

The lattice in the curved section is strong focussing with a 98° phase advance per cell and a cell length of $\sim$ 30 m. The choice was a compromise primarily dictated by intrabeam scattering considerations and a reasonable cell length which minimizes the number of quadrupoles. Typically the requirements to cope with intrabeam scattering diffusion are a small dispersion value and a relatively large betatron functions.

Each ring has a periodicity 3. Each period has a point of symmetry which we select in the middle of one of the arcs (see Fig. 9.). The structure of half of a superperiod is given by

.HSUP = .HARI .SSI .SSO .ORAH

where .HARI is the inner half arc section, .SSI is the inner long straight section which includes the dispersion killer segment and the colliding region down to the center, .ORAH is about the inverse of .HARI, and .SSO is about the inverse of .SSI with some length adjustment to compensate for the fact that the beam trajectory is on the inside of the tunnel when covering .HARI and .SSI and moves to the outside when following .SSO and .ORAH.

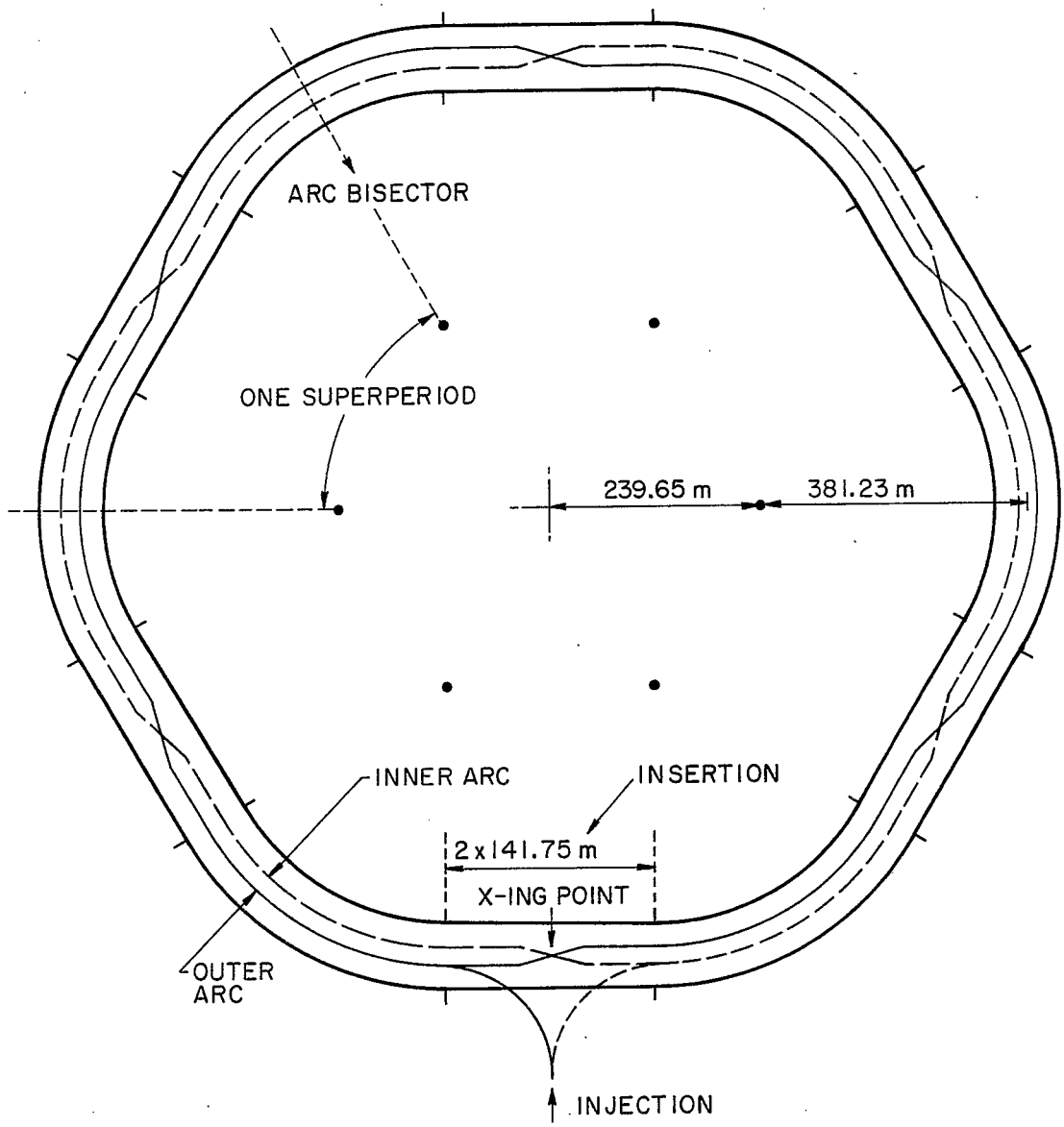

Fig. 9. Layout of the collider

The half arc sections (.HARI and .ORAH) are given by six regular cells:

.HARI = .C .C .C .C .C .C

.ORAH = inverse of .HARI

The structure of a regular cell is

.C = .FD .DF

where

.FD = QF OO B OO QD

.DF = QD OO B OO QF

A layout of a regular cell is given in Fig. 10. OO is a drift space whose length is 1.1026 m in the inner arcs and 1.1084 in the outer arcs. B is a dipole 10.7 meter long with a bending radius 275.4157 m. QF and QD are regular half-quadrupoles, 0.95 meter long with gradients

$B' / (B\rho) = 0.05610$ m for QF

$= -0.05602$ m for QD

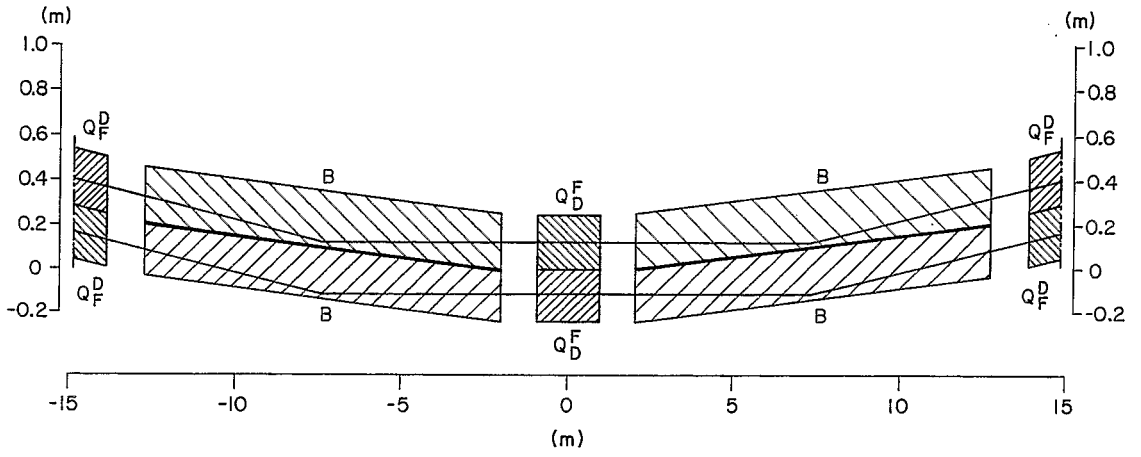

Fig. 10. RHIC regular cell pair

A kinetic energy of 100 GeV/A for gold corresponds to Bp = 839.5 T-m and, therefore, a bending field B = 3.05 Tesla.

The lattice functions in the regular cell are given in Table 8. A plot of the same functions is also shown in Fig. 11.

2. The Long Straight Sections.

Next we give the layout for the two long straight sections .SSI and and .SSO. This is also shown in Fig. 12. Both of these include a dispersion killer and a low-beta insertion. .SSI begins at the end of the regular half arc .HARI and ends at the crossing point at the end of LINS, whereas .SSO starts at the crossing point at the beginning of LINS and ends with the beginning of the regular half arc .ORAH

.SSI =	(QF)	Q8I	D78	Q7I	Q7I	D67	Q6I	Q6I	
		I562	BS	I561	Q5I	Q5I	I452	BS	
		I451	Q4I	Q4I	D34	Q3I	Q3I	D23	
		Q2I	Q2I	D12	Q1I	Q1*	DC12	BC2I	
		DC11	QC	DOC2	BC1I	LINS			
.SSO =		LINS	BC10	DOC2	QC	DC11	BC20	DC12	
		Q1*	Q10	D12	Q20	Q20	D23	Q30	
		Q30	D34	Q40	Q40	0451	BS	0452	
		Q50	Q50	0561	BS	0562	Q60	Q60	
		D67	Q70	Q70	D78	Q80			(QF)

The phase advance across each of the two halves .SSI and .SSO, including a full regular cell or each side, is exactly 1.5 π in both planes. The list of the drifts elements and of the quadrupoles are given respectively in Table 9 and 10.

BS is a dipole of a special length, 7.9037 m, used for the dispersion killing insertion and also to accommodate the ring in the geometry of the tunnel. It has the same field as the regular dipoles.

Table 8. Regular Cell Parameters

Full Length, inner arc	29.6128 m
outer arc	29.6314 m
Phase Advance/Cell	98°
β_{max}	51.6 m
β_{min}	7.5 m
η_{max}	1.39 m
η_{min}	0.64 m
Natural chromaticity/ Cell	-0.36
Local Transition Energy, γ_T (regular cell)	20.062

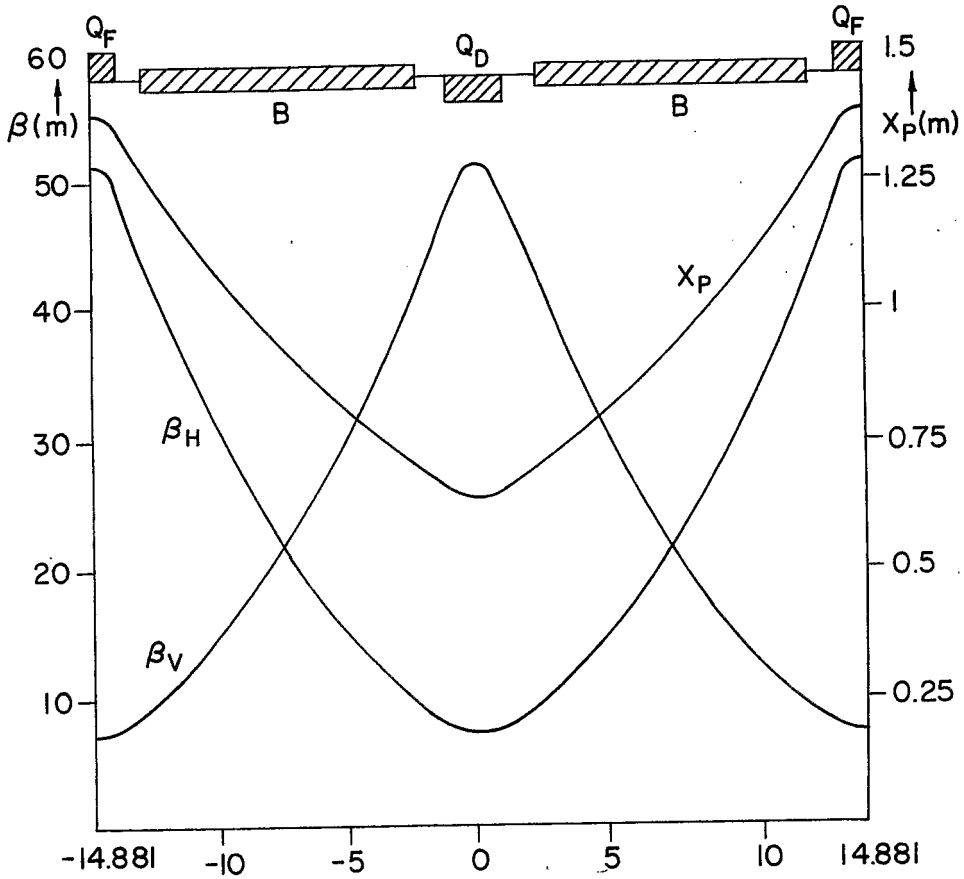

Fig. 11. RHIC regular ARC cell

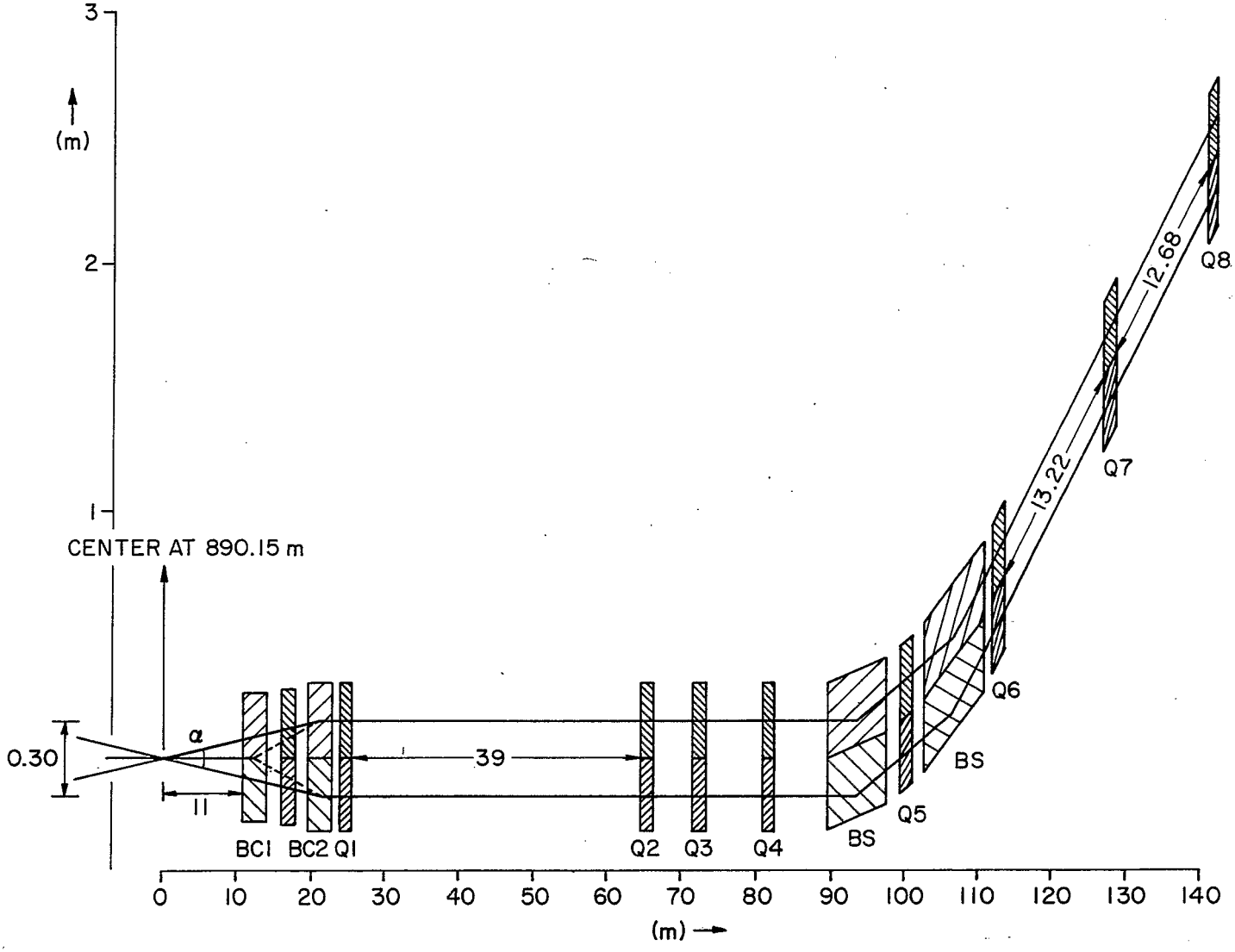

Fig. 12. RHIC half insertion

Table 9. List of the Drift Elements in the Long Straight Sections (.SSI and .SSO)

D78	12.4310 m	(*)
D67	13.2285	(**)
I562	1.0978	
I561	1.6615	
I452	1.6615	
I451	7.9289	
D34	7.8093	
D23	4.5592	
D12	38.8439	
0451	7.9333	
0452	1.6659	
0561	1.6658	
0562	1.1021	

(*) Contains Injection Kicker on the Outer Arc.

(**) Contains Injection Septum Magnet on the Outer Arc.

Table 10. List of Insertion Quadrupoles Strengths (.SSI and .SSO, Bρ= 839.5 Tm, α = 2 mrad)

Quad	$\int\frac{B'dl}{B\rho}$ (m^{-1})	$\int B'dl$ (Tesla)	Length (m)
Q_F/Q_{8I}	0.09445	79.2944	0.95 + 0.7041
Q_{7I}	0.13028	109.3727	2.5308
Q_{6I}	0.10985	92.2240	1.7308
Q_{5I}	0.11568	97.1136	1.7666
Q_{4I}	0.09855	82.7328	1.4643
Q_{3I}	0.14135	118.6652	2.2791
Q_{2I}	0.10593	88.9269	1.4826
$Q_{1I}/Q1^*$	0.02895	24.3045	1.4976
Q_C	0.13340	111.9858	2.0076
Q_C	0.13340	111.9058	2.0076
$Q_{1O}/Q1^*$	0.0289	24.2726	1.4976
Q_{2O}	0.10584	88.8533	1.4826
Q_{3O}	0.14124	118.5735	2.2791
Q_{4O}	0.09851	82.6959	1.4643
Q_{5O}	0.11573	97.1534	1.7666
Q_{6O}	0.10984	92.2124	1.7300
Q_{7O}	0.13032	109.4054	2.5308
Q_{8O}/Q_F	0.09444	79.2839	0.07041 + 0.95

The two halves of the long straight sections have slightly different lengths to compensate for the beam moving from the inner to the outer portion of the ring. The lengths are

$$\begin{aligned} .SSI &= 141.7459 \text{ m} \\ .SSO &= 141.7631 \text{ m} \end{aligned}$$

The overall lattice functions are shown plotted in Fig. 13 for a crossing angle of 2 mrad.

The regions between the end of the second of the special dipole (BS) and the front of the first of the dipoles that bring the two beams to a crossing (BC2I or BC2O) have zero dispersion.

3. The Colliding Regions

The colliding regions have the following elements

(Q1*)	DC12	BC2I	DC11	QC	DOC2	BC1I	LINS	
	LINS	BC1O	DOC2	QC	DC11	BC2O	DC12	(Q1*)

There is a magnet free space (LINS LINS) of +/- 11 meters.

The lattice parameters at the crossing point are (for α = 2 mrad)

$$\begin{aligned} \beta_H^* &= 0.88 \text{ m} \\ \beta_V^* &= 6.3 \text{ m} \\ \alpha_H^* = \alpha_V^* &= 0.0 \\ \eta^* &= 0.0 \text{ m} \end{aligned}$$

The unusual difference in the β^*-values in the two planes is due to the condition imposed that the β_{max} value will not exceed $\sim$315 m in both planes (see Fig. 13).

There are two pairs of horizontally bending magnets BC1 and BC2 to bring the two beams into collision. There are two possible configurations.

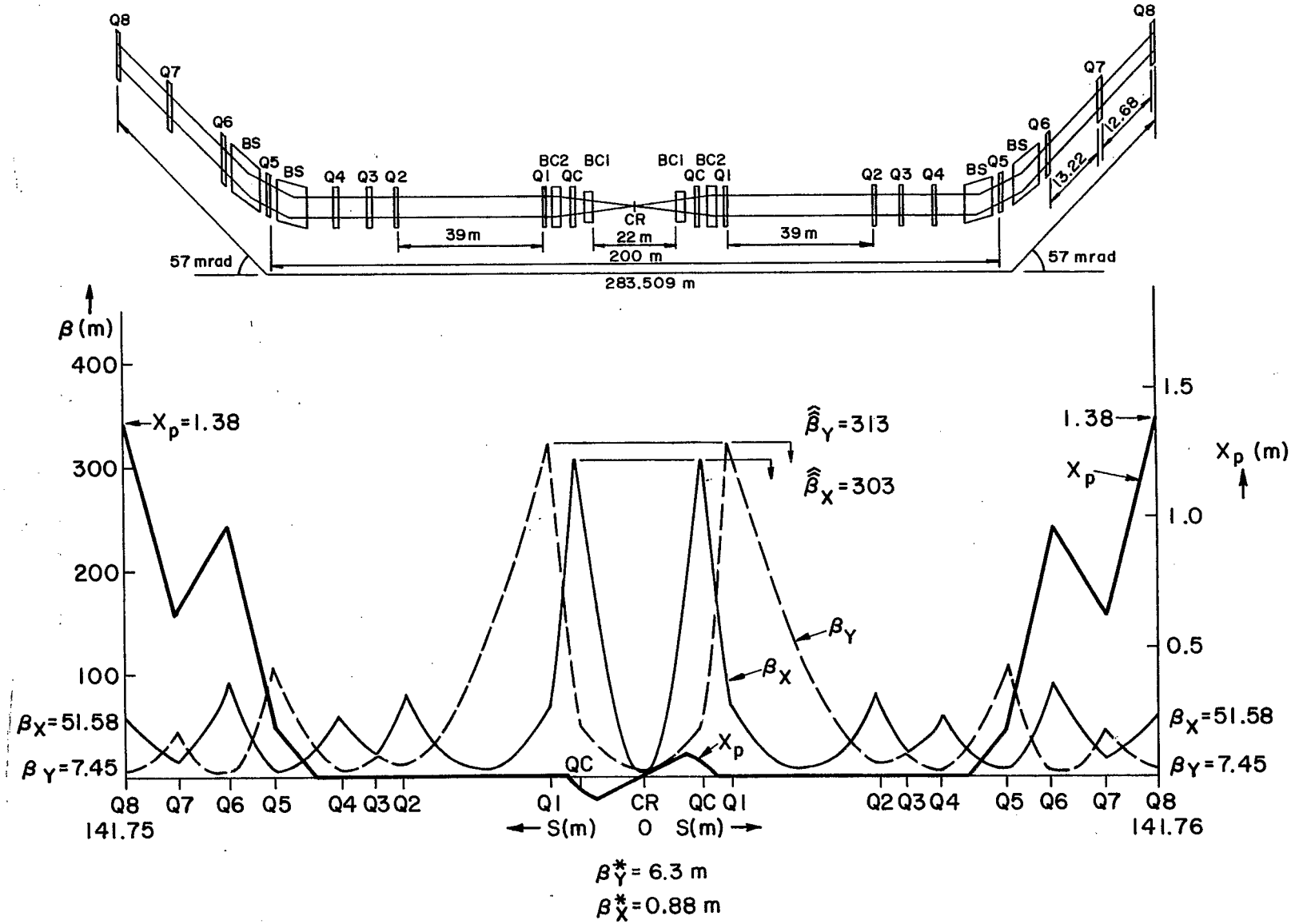

Fig. 13. Insertion for RHIC

(i) Crossing at Large Angle (α = 2 mrad). This has been our reference design and it is shown in Fig. 14(a). The magnet parameters are given in Table 11. The luminosity is lower than for $\alpha = 0$, but the length of the interaction region is shorter.

(ii) Head-on Collision ($\alpha = 0$). This mode of operation corresponds to the largest luminosity and the longest interaction region. The geometry is shown in Fig. 14(b). The magnet length and strength are given in Table 11. The lattice value, at the crossing point for this case do not change appreciably ($\beta_H^* = 0.94$ m and $\beta_V^* = 6.3$ m) and the overall behaviour is very similar to that shown in Fig. 13. Nevertheless, this insertion cannot be derived from the former by simply readjusting the currents in the magnets, but requires moving them physically.

Observe that although the innermost dipole BC1 is common to both beams, this will not preclude the operation of the collider with beams of unequal species or different energies.

Because of the dipoles inserted to bring the two beams into collision, we have placed the first quadrupoles (QC) about 16 meters from the crossing point. These quadrupoles have the dual function of making the dispersion zero and providing a low beta value at the crossing point. This still causes the inconvenience of a large beta-value in proximity to both QC and Q1. We have been able to keep this value to $\sim$310 m in both planes (see Fig. 13) for the large angle crossing and $\sim$350 m for head-on collisions. The maximum values occur in QC and Q1.

4. Beam Acceleration and RF Considerations

As we have already explained, the rf harmonic number ought to be an integer times 57, and the integer cannot be larger than 12, the limitation being

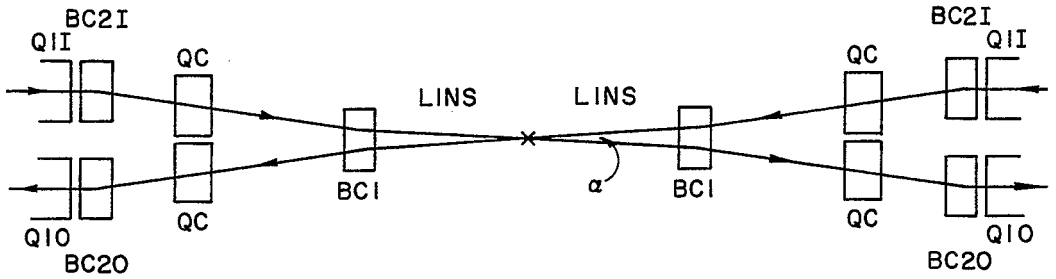

Fig. 14a. Crossing at an angle, α.

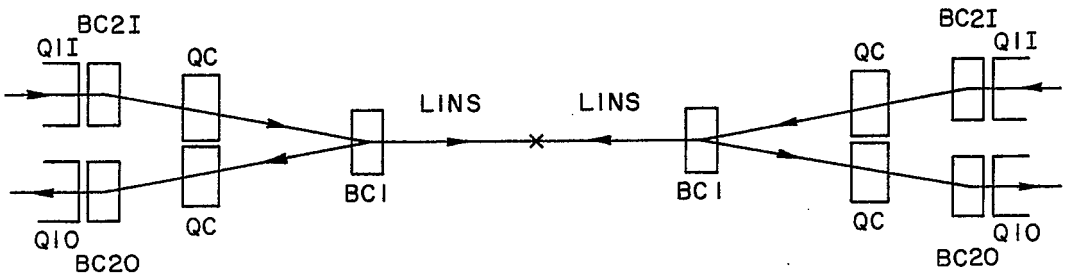

Fig. 14b. Head-on collision, $\alpha = 0$

Table 11. Parameters for Dipoles at the Crossing Point Regions. (30 cm beam separation, $B\rho$ = 839.5 T.m.)

Crossing Angle	Dipole Number	Length (m)	Deflection (mrad)	Bend Radius (m)	Field at γ = 100 (Tesla)
α = 0	BC1I	3.00	16.901684	177.5	4.729
	BC1O	3.00	-16.901684	177.5	4.729
	BC2I	3.207	-16.901684	189.8	4.424
	BC2O	3.207	16.901684	189.8	4.424
α = 2 mrad	BC1I	3.00	14.493373	207.00	4.05558
	BC1O	3.00	-14.493373	207.00	4.05558
	BC2I	3.207	-15.493373	207.00	4.05558
	BC2O	3.207	15.493373	207.00	4.05558

caused by the length of the rf buckets which have to capture the bunches from the AGS. On the other hand, the choice of a high frequency would allow shorter bunches in the colliding beam mode. For crossing at an angle, shorter bunches enhance the luminosity, whereas for head-on collision they make small interaction regions, an important requirement for particle detector design. We have compromised and chosen the harmonic number h = 6x57 = 342 which corresponds to an rf frequency of 26.743 MHz (for $\beta = 1$).

A peak rf voltage of 1.2 MV is necessary for the acceleration of the beam and to provide reasonably large rf buckets in the storage mode. We take 60 sec to accelerate the beam from injection to top energy. The energy gain per turn for the different ion species is given in Table 12, where we also give the bucket area and height without acceleration at injection and at the top energies corresponding to B ρ = 839.5 Tesla-meter, with a transition energy $\gamma_T = 26.4$ and a constant voltage of 1.2 MV. The synchronous angle is given by $\sin \theta_s = 0.048$, assuming a linear ramp at constant rf voltage. For a moving bucket during acceleration the area is obtained by multiplying the value in Table 12 by $\alpha = 0.9$, and the height by $Y/\sqrt{2}$ where Y = 1.36.

Since at injection the bunch area is 0.3 eV•sec/A for all species, one can see that the buckets have enough area and height.

In Table 12 we also give the full (+/- 95%) bunch length and height of the beam at the transition energy crossing, assuming a full voltage of 1.2 MV. These quantities have nevertheless been calculated for a full bunch area of 1.0 eV•sec/A. In fact it has been found that the beam bunches suffer a coherent microwave instability when crossing the transition energy; this is caused by the smallness in that region of the parameter $\eta = \gamma^{-2} - \gamma_T^{-2}$ which provides Landau damping for the stability.

Table 12. Beam Acceleration and RF buckets Parameter

	Proton	Deuterium	Carbon	Sulfur	Copper	Iodine	Gold
Energy Gain/Turn, KeV/A	47.5	23.7	23.7	23.7	21.9	19.8	19.1
Stationary bucket area:							
Injection	21.7	3.3	3.4	3.4	2.7	2.2	2.0
Top energy, eV•sec/A	29.9	15.2	15.2	15.2	13.9	12.8	12.2
Bucket half-height:							
Injection	1.58	0.481	0.487	0.489	0.431	0.376	0.356
Top energy Δ p/p, %	0.250	0.254	0.254	0.254	0.255	0.256	0.256
Bunch height @ transition Δ p/p full (%)	1.41	1.26	1.27	1.27	1.25	1.23	1.22
Bunch length @ transition full (nsec)	1.05	1.18	1.18	1.18	1.20	1.22	1.23
Characteristic time of transistion energy crossing msec	15.4	24.5	24.3	24.3	25.7	27.4	28.2

γ_T = 26.4 harmonic number = 6 x 57 = 342
RF Frequency (β =1) = 26.743 MHz
Total RF voltage = 1.2 MV
Acceleration period = 60 seconds
RF Phase Angle, θ_s = 2.3°

A simple phenomenological model has been proposed and the analysis of the instability worked out numerically. In this model the beam bunch is assumed to take the shape as required only by the external rf voltage and remains otherwise unmodified as it goes through the transition energy. The growth rate of the instability is then calculated locally for a given impedance, Z/n (complex), and integrated over the whole crossing. The growth rate is estimated by solving numerically the dispersion relation for the instability assuming a gaussian for the energy distribution. The growth rate depends on the choice of the harmonic number n which, considering the short length of the bunches, has been taken in proximity of the beam pipe cut-off ($\sim 2 \times 10^4$).

According to our model the maximum bunch growth factor depends crucially on the parameter

$$N_B \, |Z/n| \, Q^2/A \qquad (5)$$

where N_B is the number of particles per bunch, Q the charge state and A the atomic mass.

The results are shown in Figs. 15 and 16 for gold, which give the upper limit of the estimate respectively of the local growth rate and of the total bunch area growth for a few initial values of the bunch area on which they have a strong dependence. Assuming $|Z/n| \sim 5$ ohm, with 1.1×10^9 particles per bunch, we expect for gold a bunch area increase to no more than 1.0 eV·sec/A.

One important parameter, which determines the bunch shape when crossing the transition energy, is a characteristic time, also given in Table 12, during which the motion is "non-adiabatic." There is another related effect that has been investigated. This is the mismatch of the longitudinal space

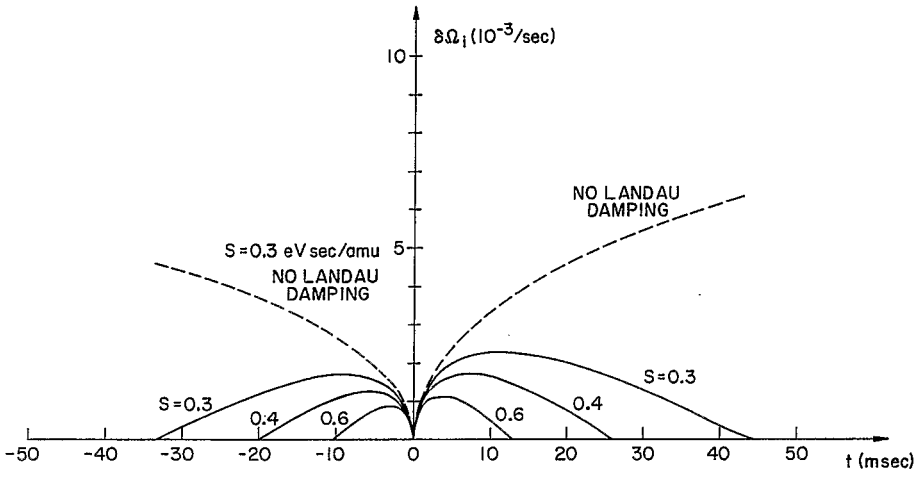

Fig. 15. Microwave instability growth rate upper limit estimate when crossing transition energy

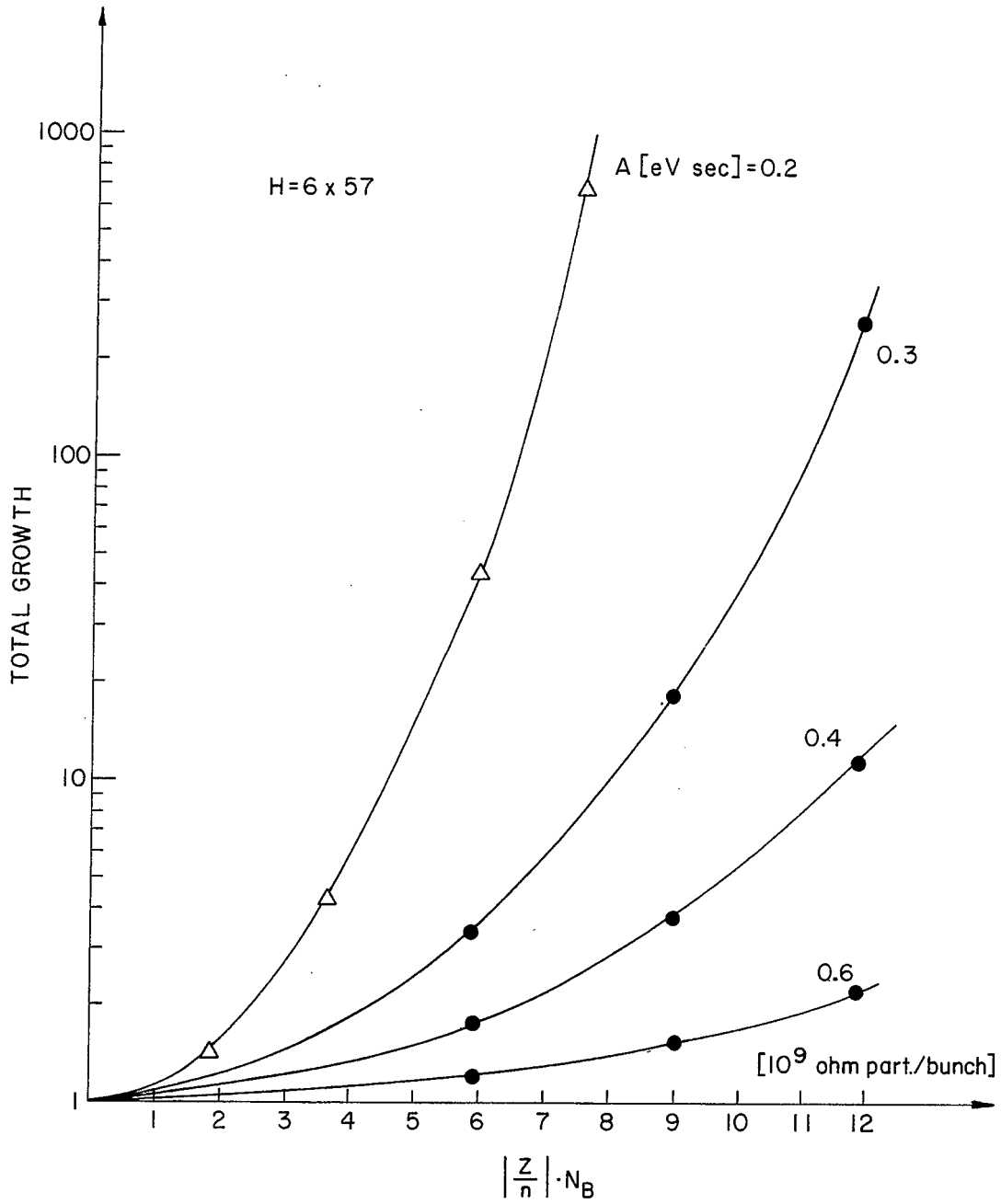

Fig. 16. Maximum bunch area growth due to microwave instability when crossing the transition energy

charge forces with the external rf forces. This effect has been found to be quite negligible.

In the colliding beam mode, especially for the case of gold on gold at top energy, the rf voltage must be 1.2 MV to provide a bucket large enough to contain the particle bunches after being in the collider for several hours and have experienced growth from intrabeam scattering (next section).

The rf system has six cavities in each ring of the Collider. One is shown in Fig. 17. Each cavity is about 2.5 meter long and provides 200 kV. The gap is 4 cm wide and the bore has a radius of 3 cm. The outer dimension is a radius of about 25 cm to allow a beam separation of 30 cm. The estimated shunt impedance (from the wall alone) is $\sim$5.4 Mohm which corresponds to a dissipated power of 17 kW. Each cavity will be connected to its own individual amplifier, capable of 25 kW, to allow for transmission efficiency.

For gold the electric current in the beam is 65 mA-electric and, considering the large shunt impedance, the beam itself is capable of inducing about 0.5 MV, half of the total required. This is an acceptable situation, but care must be taken to compensate dynamically for beam loading.

An inspection of Table 7 shows that the amount of frequency tuning during the acceleration cycle is quite small, no more than 3.2% for gold, and this can be achieved mechanically.

5. Intrabeam Scattering

This is the phenomenon by which particles in the same bunch exchange longitudinal and transverse momenta by Coulomb scattering. This effect depends strongly on the charge Ze and on the mass number A of the ions. The scattering is proportional to

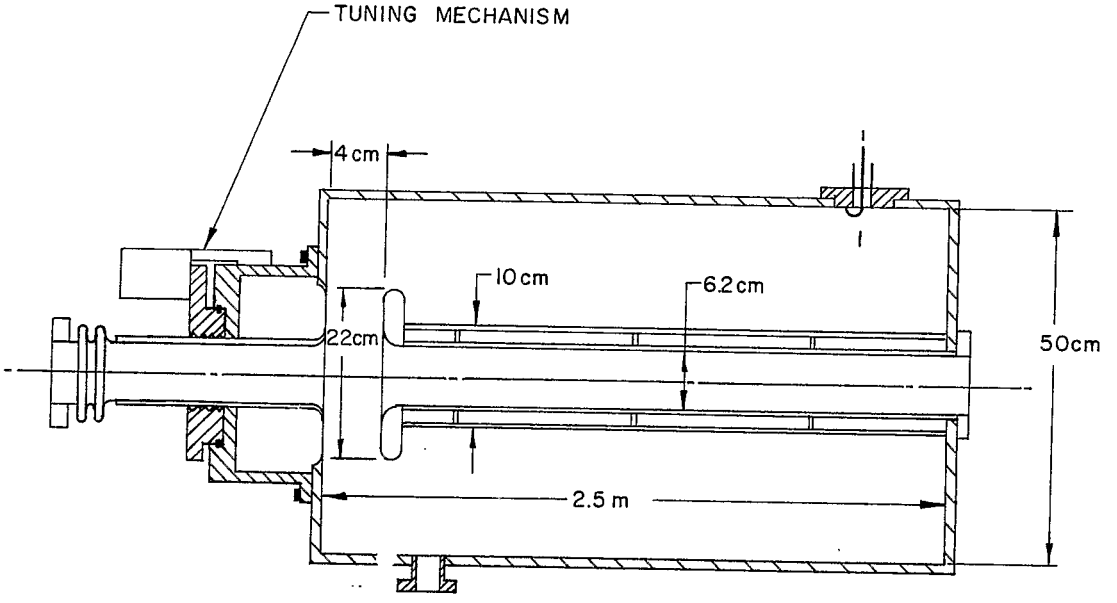

Fig. 17. RHIC RF cavity unit

Z^4/A^2.

For very heavy ions we clearly expect a severe limitation from intrabeam scattering.

The diffusion rates caused by this effect depend linearly on the beam density in the 6-dimensional phase space and on a form factor which is a rather complicated function of the lattice parameters, beta values, dispersion, and on the relative spread in the velocities.

We have made computer estimates of the diffusion rates for the lattice of the Collider specified in the previous chapters of this note, including the long straight sections. Theories do exist (Piwinsky and Bjorken and Mtingwa) which can be used to estimate the growth rates of the three dimensions of a bunch at a particular location of the lattice, and several computer codes are available for this task. A model has been created to estimate the growth rates averaged over the entire circumference of the lattice. For this purpose magnet and drift lengths have been taken into account. Moreover, actual variations of the lattice functions α_H, α_V and η' have also been properly handled.

If the two modes of oscillation are taken to be completely decoupled, typically one finds that the horizontal mode has a positive growth whereas the vertical oscillations are damped, though usually at rather small rates. This fact would quickly convert the initially assumed "roundness" of the beam to an extreme "flatness." Because both linear and non-linear coupling are inherent in the Collider, and with the assumption that the coupling has time periods shorter than the intrabeam scattering diffusion time, we assume that the beam is capable of remaining round; i.e., that the horizontal and vertical beam emittance are always equal. Their common value is allowed to diffuse at a rate given by the algebraic sum of the diffusion rates for the two modes of oscillation.

The instantaneous and local diffusion rates are proportional to the bunch peak current, given by

$$I_P = \frac{N_B e \beta c}{\sqrt{2\pi}\ \sigma_\ell}, \tag{6}$$

where N_B is the number of particles per bunch (see Table 7) and σ_ℓ the rms bunch length. As the beam diffuses the bunch dimensions increase and the diffusion rates correspondingly decrease. This fact has been taken into account in our estimates.

The result given here is for gold since we believe this to be the worst case. In Fig. 18 we give the rms momentum spread of the bunch versus the beam energy in units of γ at the end of a two-hour and ten-hour storage periods. As shown in Fig. 18, for $10 \lesssim \gamma \lesssim 100$, the growth can easily be contained within the rf bucket dimensions.

In Fig. 19 we give similar results for the rms bunch length. Bunches quickly become long at the low energy end.

As initial values, we have taken a bunch area of 0.3 eV•sec/A for $\gamma < \gamma_T$ and a value of 1.0 eV•sec/A for $\gamma > \gamma_T$ to take into account the bunch growth from the microwave instability when crossing the transition energy. For the betatron emittance we have always assumed, at any energy, the same initial value of 10 π-mm-mrad (normalized emittance, 95% of the beam).

The emittance growth (the same in both planes, because of our assumption of full coupling) is shown in Fig. 20. A remarkable result is that the beam behaviour for $\gamma > \gamma_T$ is independent of γ, whereas for $\gamma < \gamma_T$ the growth rate increases quickly as the beam energy decreases. It is not easy to understand the behaviour for $\gamma < \gamma_T$. But for $\gamma > \gamma_T$ the result is predicted by the

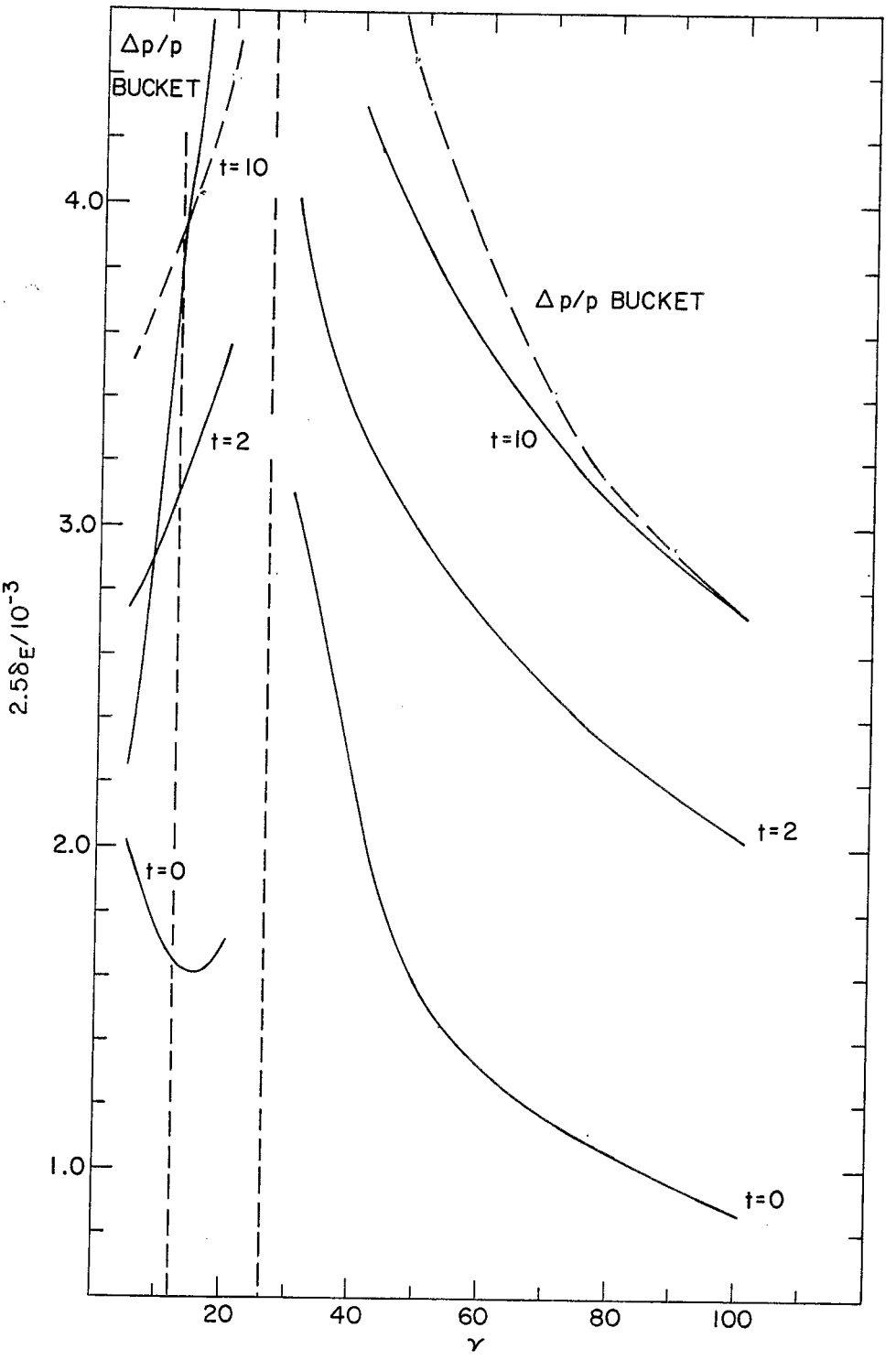

Fig. 18. Beam bunch height growth due to intra beam scattering

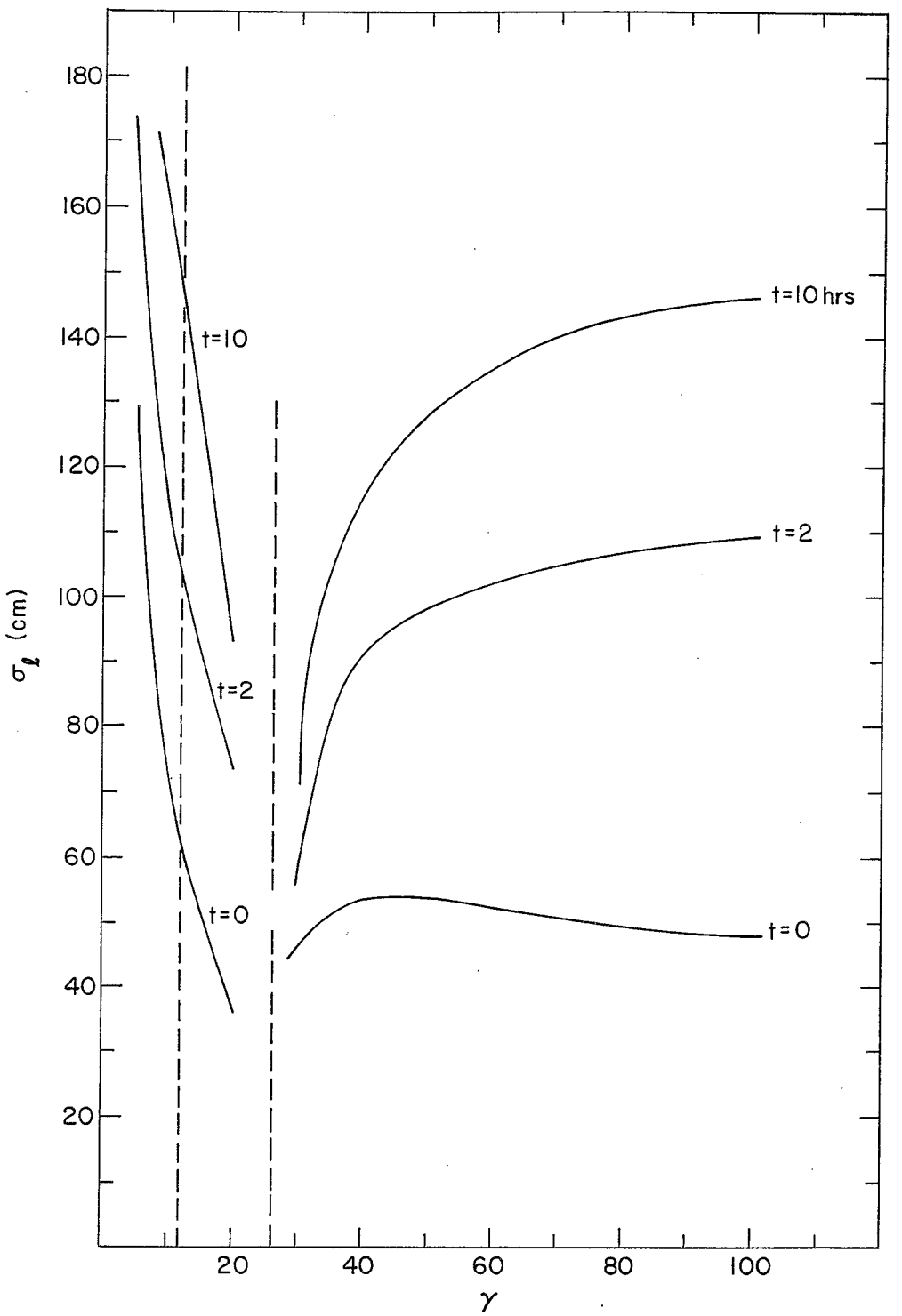

Fig. 19. Bunch length growth due to intra beam scattering

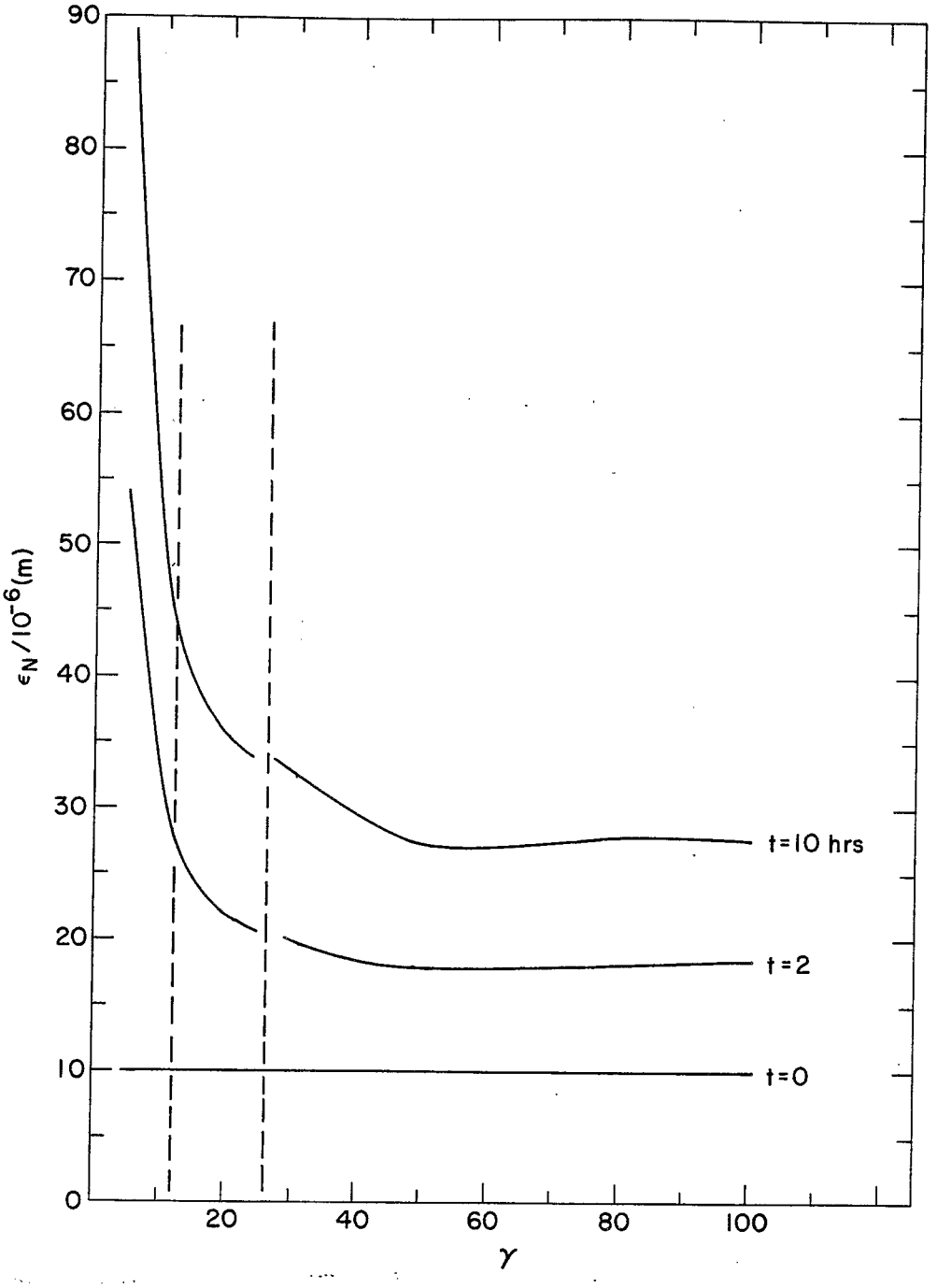

Fig. 20. Beam emittance growth due to intra beam scattering

theory. Moreover, in this case larger values of γ_T would yield lower growth rates about linearly.

Finally in Fig. 21 we give the overall beam dimensions versus energy at the end of two-hour and ten-hour storage periods. These are the maximum values estimated in the center of the quadrupoles in the regular lattice (the arcs) of the Collider. They are half of the full dimensions in the horizontal plane, obtained with the equation

$$\sqrt{6}\,\sigma_E + 6\,\sigma_\beta$$

where σ_E is the rms contribution from the momentum spread and σ_β is the rms contribution from betatron oscillations. The lattice values used in estimating the beam dimensions are

$$\begin{aligned} \beta_{max} &= 51.6 \text{ m} \\ \eta_{max} &= 1.39 \text{ m} \end{aligned} \qquad (7)$$

Whereas the beam dimension varies at most by a factor two between $\gamma = 20$ and $\gamma = 100$, there is a rather steep increase of the beam size for smaller energies.

6. Magnet Considerations, Numbers, and Aperture Requirements

Table 13 gives the statistics for all magnets of the two Collider rings. The parameters given correspond to a magnetic rigidity,

$$B\rho = 839.5 \text{ Tesla-meter} ,$$

a kinetic energy of 100 GeV/A for gold. The special dipoles in the colliding region for bringing the two beams into collision have been listed in Table 11.

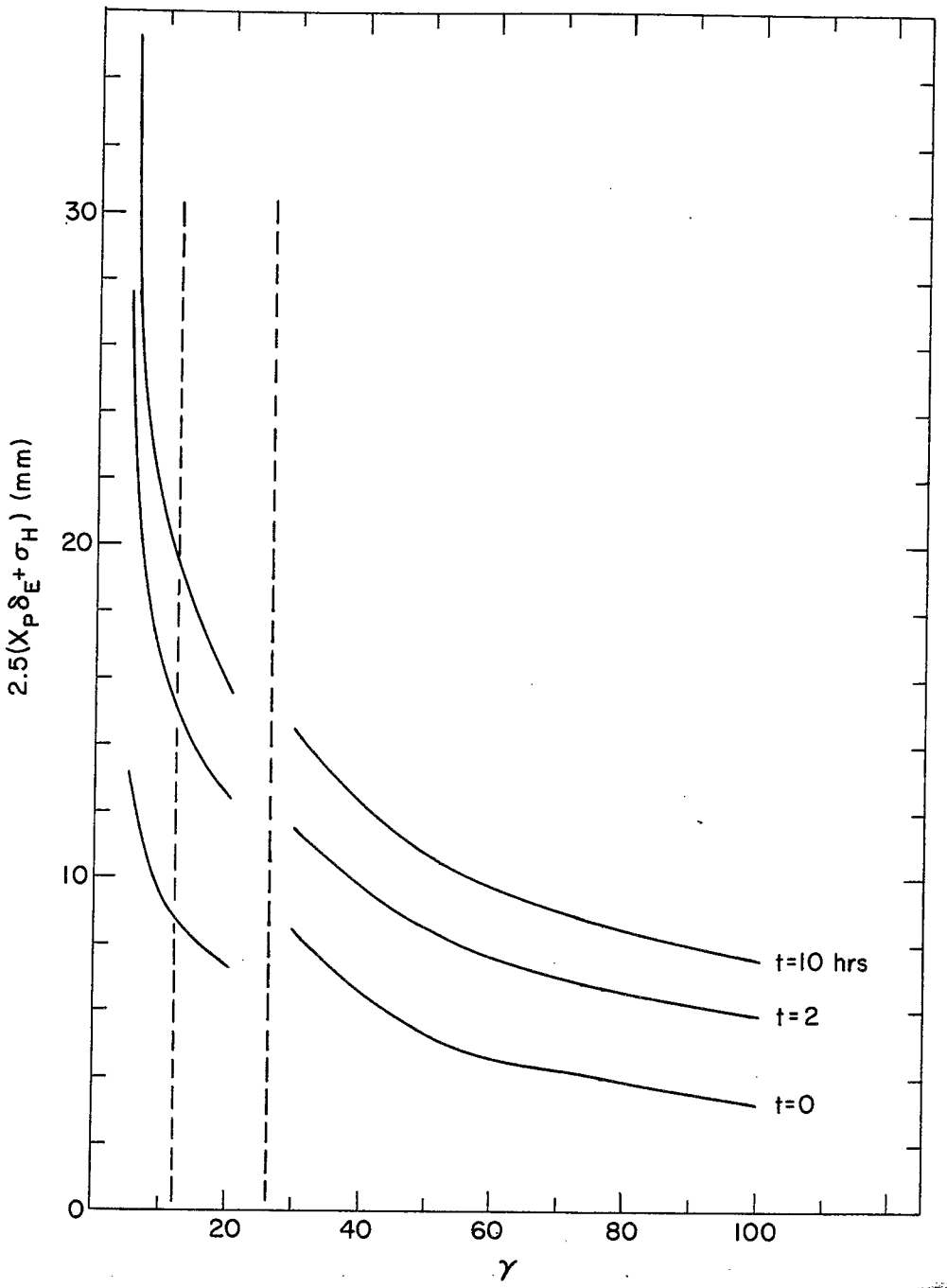

Fig. 21. Beam half-width growth due to intra beam scattering

Table 13. Magnet Statistics

Dipoles (**)

Kind	B	BS
Magnetic Length, m	9.32	7.9037
Field, Tesla	3.5	3.5
Bending Radius, m	239.9	239.9
Bending Angle, mrad	38.85	32.95
Sagitta, cm	4.6	3.3

Number of dipoles (180 dual + 12 single) = 192

Quadrupoles

Magnetic Length (*)		1.20 m
Gradient		76.3 T
Number of quadrupoles (dual)		
	Arcs	138
	L.S. Insertion	108
	Total/Ring	246

(*)For the quads in the arcs. For those in the long straight sections use Table 9.

(**)Special dipoles to bring the two beams in collison are not included in this list. See Table 11.

The largest beam dimensions in the arcs for the case of gold are given in Table 14 at injection, transition and top energy. The values correspond to two hours storage time for injection and ten hours for the top energy case and have been taken from Figs. 18 and 20 with the the lattice values given by (7). The energy spread at transition is taken from Table 12. The dimensions are for 95% of the beam, the width (a_H) has been calculated by taking the linear combination of the contributions from momentum spread and betatron oscillations (a_v). The largest beam dimensions are at the transition energy or at injection as expected. For the lighter ions one can assume similar values or smaller.

The criterion chosen for the aperture of the magnet is the following. The "good field" region of either quadrupoles or dipoles should be large enough to contain a beam dimension calculated according to the formula

$$6\ \sigma_\beta + \sqrt{6}\ \sigma_E = (\sqrt{6} - 1)\ a_v + a_H$$

where σ_β and σ_E are respectively the rms contribution to the total beam dimensions from betatron oscillations and energy spread. The dimensions a_v and a_H are given in Table 14. This requirement must apply for blown-up beam dimensions after at least ten hours of storage for $\gamma \geq 30$. The dimensions for $\gamma = 30$ are therefore also shown in Table 14.

As expected the limit is set at $\gamma = 30$. Including also a possible closed orbit distortion of ± 2mm, the "good field" region requirement for the magnets has been taken to be

$$\pm\ 26\ \text{mm}$$

The "good field" region is defined here as that region around the centre of the magnet where the magnet imperfections do not exceed some value. For example, for the dipoles, the field error $\Delta B/B$ is to be kept below the

Table 14. Maximum Beam Dimensions (95%) for Gold in the Regular Quads (Arcs)

Injection (γ = 12.0)			
ε_N	(normalized emittance)	27.4 π mm-mrad	(after two hours)
ε	(actual emittance)	2.28 π mm-mrad	
a_v	(half-height)	10.8 mm	
$\Delta p/p$	(momentum spread)	3.0×10^{-3}	(after two hours)
a_H	(half-width)	15.0 mm	
Transition (γ = 26.4)			
ε_N		10 π mm-mrad	(in acceleration mode)
ε		0.38 π mm-mrad	
a_v		4.4 mm	
$\Delta p/p$		12.2×10^{-3}	(in acceleration mode)
a_H		21.4 mm	
Top Energy (γ = 100)			
ε_N		27.8 π mm-mrad	(after ten hours)
ε		0.278 π mm-mrad	
a_v		3.78 mm	
$\Delta p/p$		2.7×10^{-3}	(after ten hours)
a_H		7.5 mm	
Low Energy (γ = 30)			
ε_N		33.2 π mm-mrad	(after ten hours)
ε		1.1 π mm-mrad	
a_v		7.5 mm	
$\Delta_{p/p}$		4.9×10^{-3}	(after ten hours)
a_H		14.3 mm	

2×10^{-4} level in that region. This criterion excludes those dipole, quadrupole, and sextupole errors which can be coped with either using special correcting coils or by taking them into account for the orbit analysis.

For the magnets being considered it is expected that the ratio between the "good field" region and the coil i.d. could be 2/3 or even better. The coil i.d. is 75.4 mm and the vacuum chamber internal diameter is 65.4 mm.

At $\gamma = 20$ the criterion is satisfied for only two hours of storage time. At injection ($\gamma = 12$) some beam losses are to be expected for two hour storage. Finally the colliding beam mode of operation near the transition energy will be avoided. In the acceleration mode, the 95% beam dimensions when crossing the transition energy can easily be accommodated within the magnet aperture.

The aperture requirements for the magnets in the long straight sections have to be examined with a different strategy. The beam envelopes are given in Figs. 22, 23, 24, 25 and 26 for different energies and locations around the lattice of the Collider. The dimensions shown correspond to 6 times the rms beam size from betatron oscillations centered around the two extreme off-momentum orbits for $\sqrt{6}$ times the beam rms momentum spread. With the exception of injection and transition energy, the dimensions correspond to 10 hours of storage and 2 hours for $\gamma = 12.5$.

The lattice behavior in the long straight sections is shown in Fig. 13. As far as the quadrupoles are concerned the β-values could be too large, especially for those labelled Q1 and QC in both inner and outer halves. At their location $\beta \sim 310$ m but fortunately the dispersion is zero and we can ignore the contribution to the beam size from the momentum spread. These quadrupoles should have a larger aperture than the others, corresponding to a "good field"

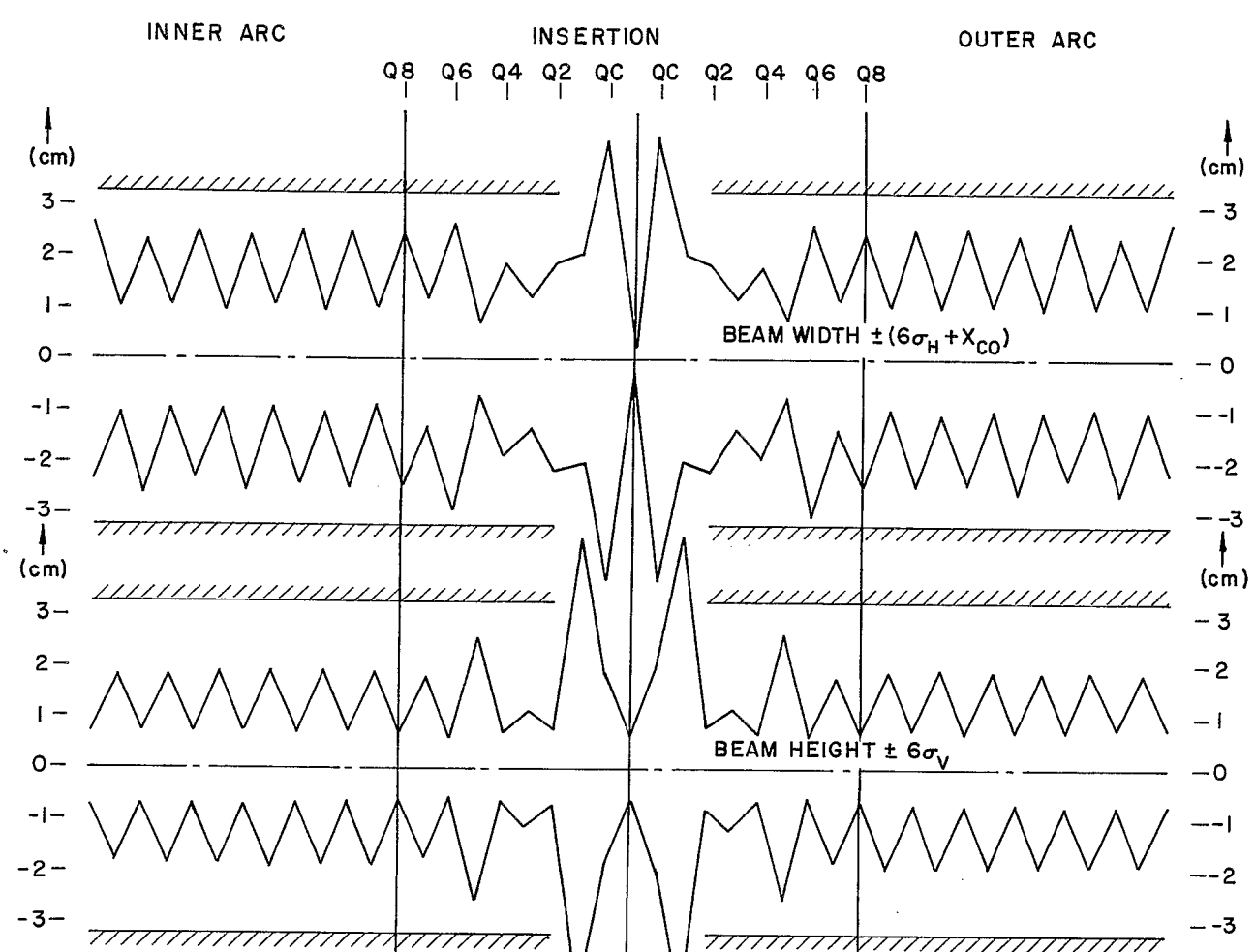

Fig. 22. Width and height of the Au beam and injection ($\gamma = 12$, $\varepsilon_N = 10 \times 10^{-6}$ π rad-m, $\Delta p/p \pm 1.7 \times 10^{-3}$)

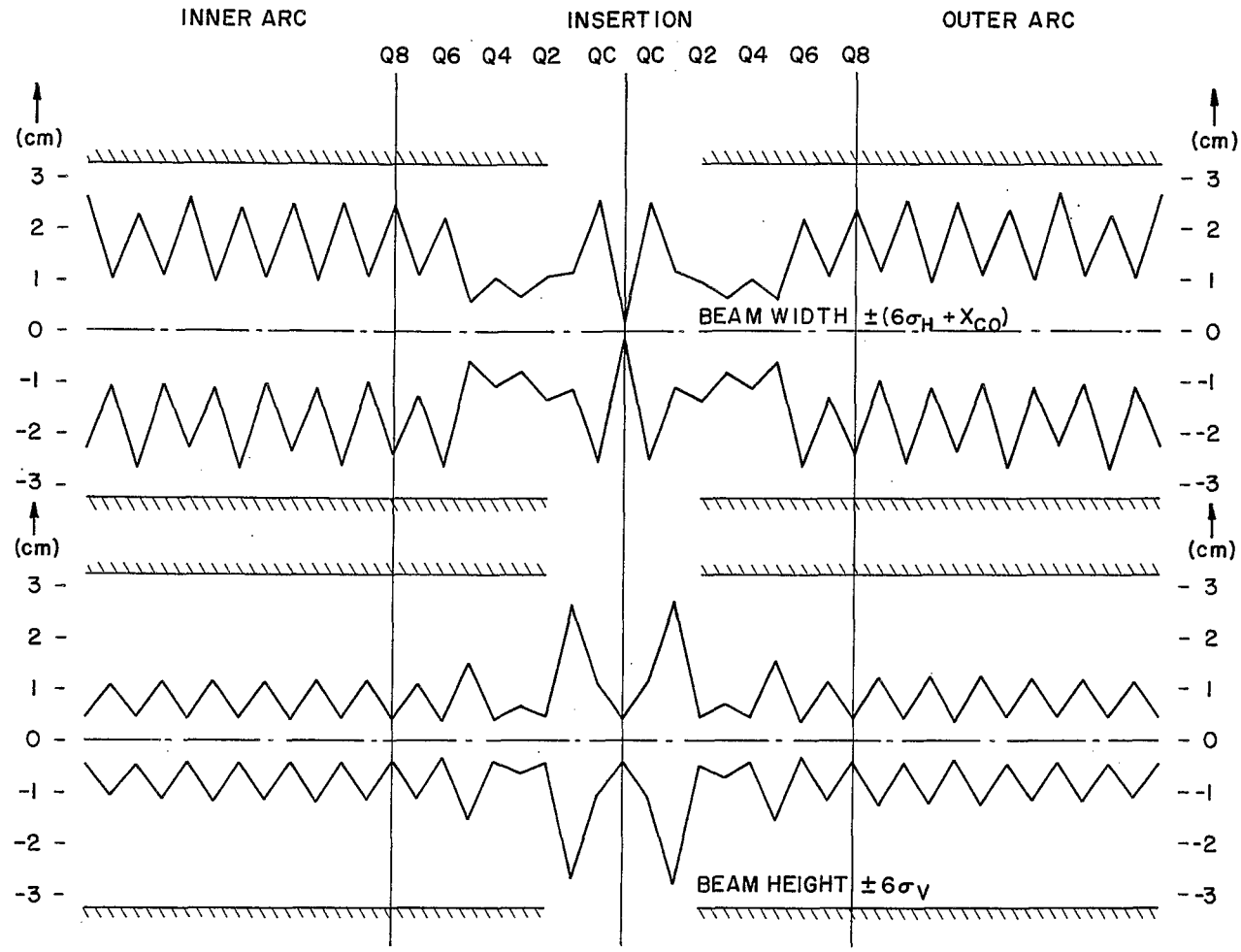

Fig. 23. Width and height of the Au beam when passing through transition (γ = 26.4, ε_N = 10 x 10^{-6} π rad-m, $\Delta p/p \pm 0.01$)

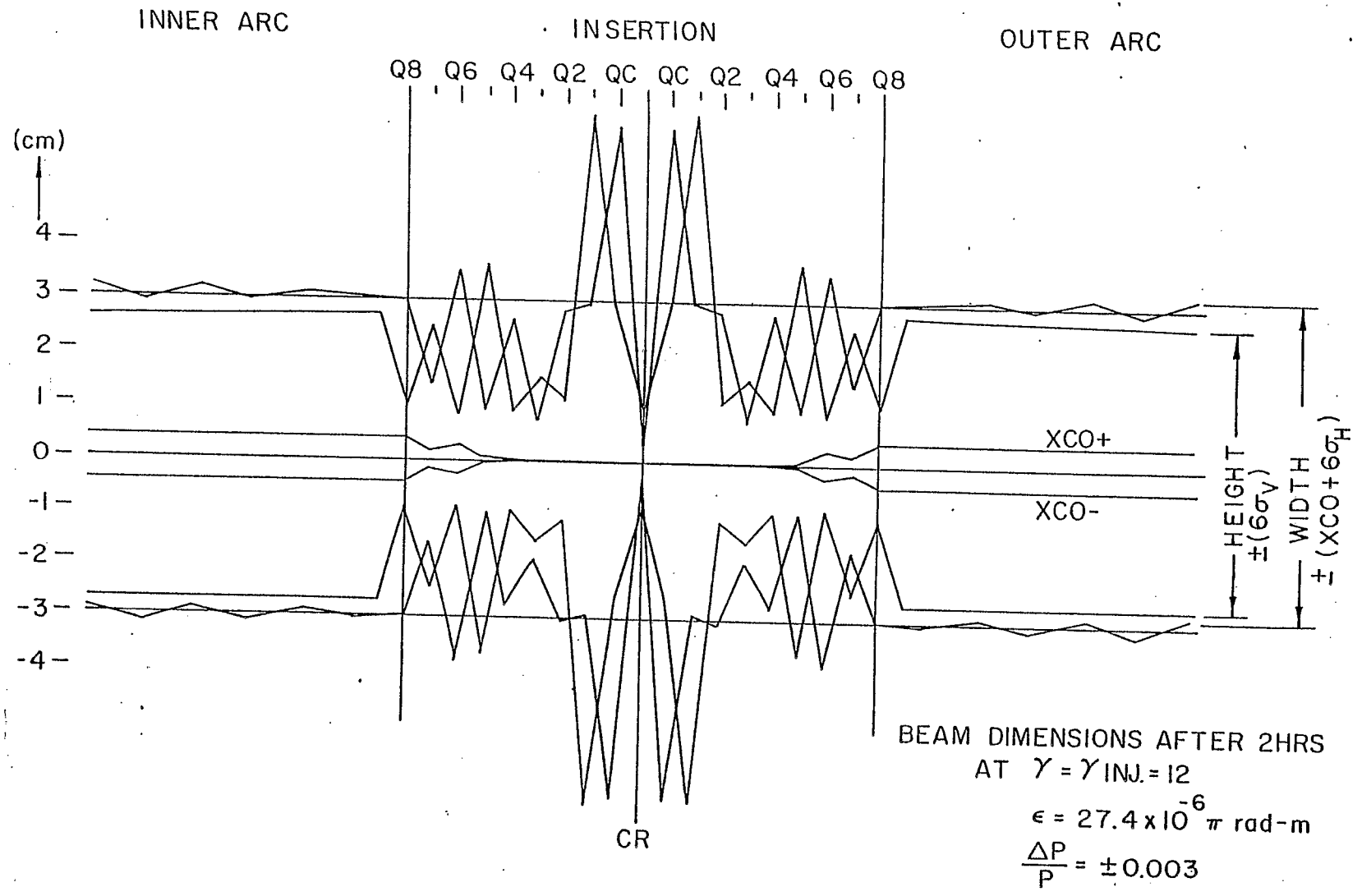
INNER ARC
INSERTION
OUTER ARC
Q8 Q6 Q4 Q2 QC QC Q2 Q4 Q6 Q8
(cm)
4
3
2
1
0
-1
-2
-3
-4
XCO+
XCO-
HEIGHT ±(6σV)
WIDTH ±(XCO+6σH)
CR
BEAM DIMENSIONS AFTER 2HRS
AT γ = γ INJ. = 12
ε = 27.4 x 10^-6 π rad-m
ΔP/P = ±0.003

Fig. 24.

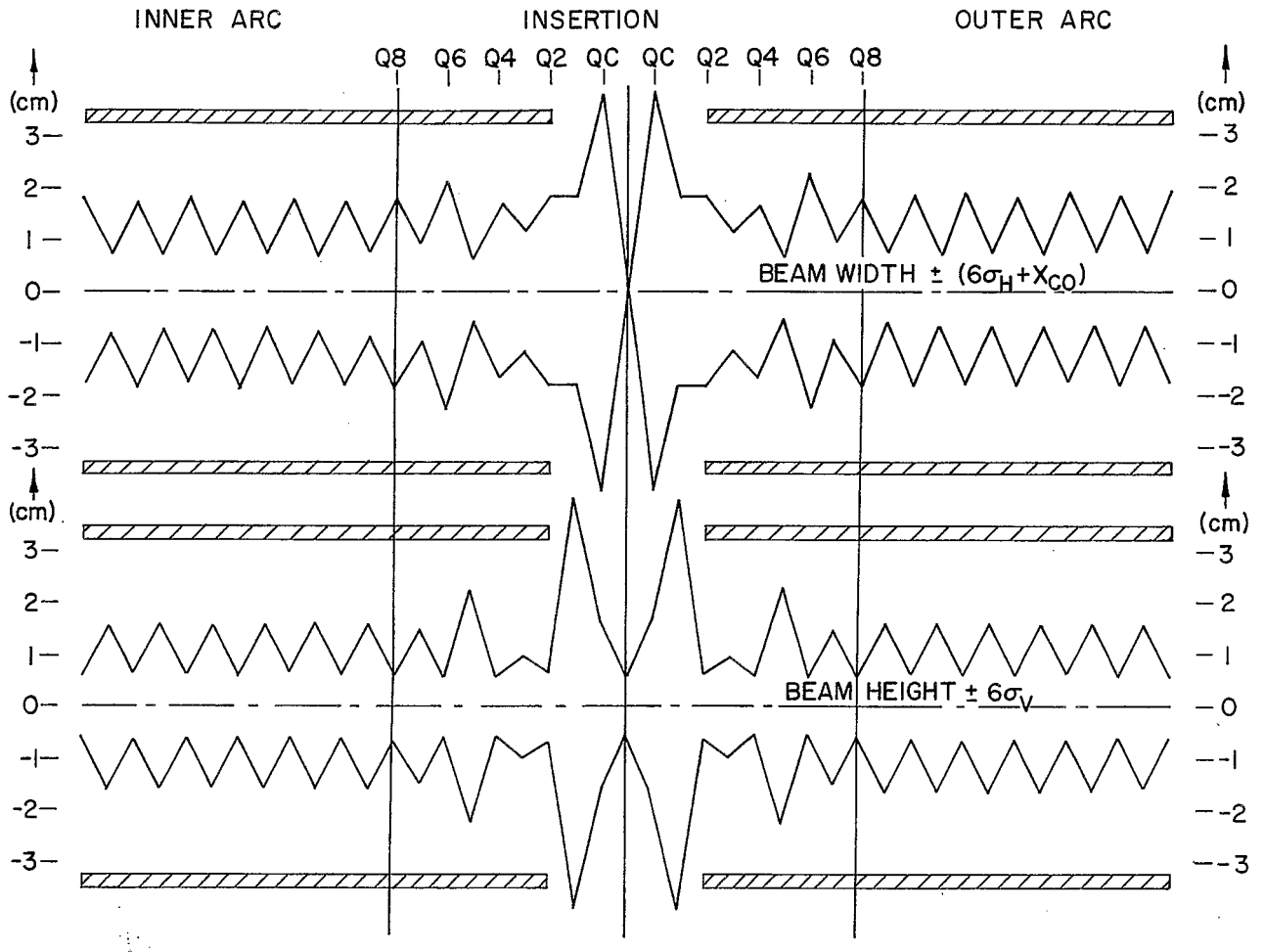

Fig. 25. Width and height of the Au beam after 10 hours at $\gamma = 30$ ($\varepsilon_N = 33.2 \times 10^{-6}$ π rad-m, $\Delta p/p \pm 5.0 \times 10^{-3}$)

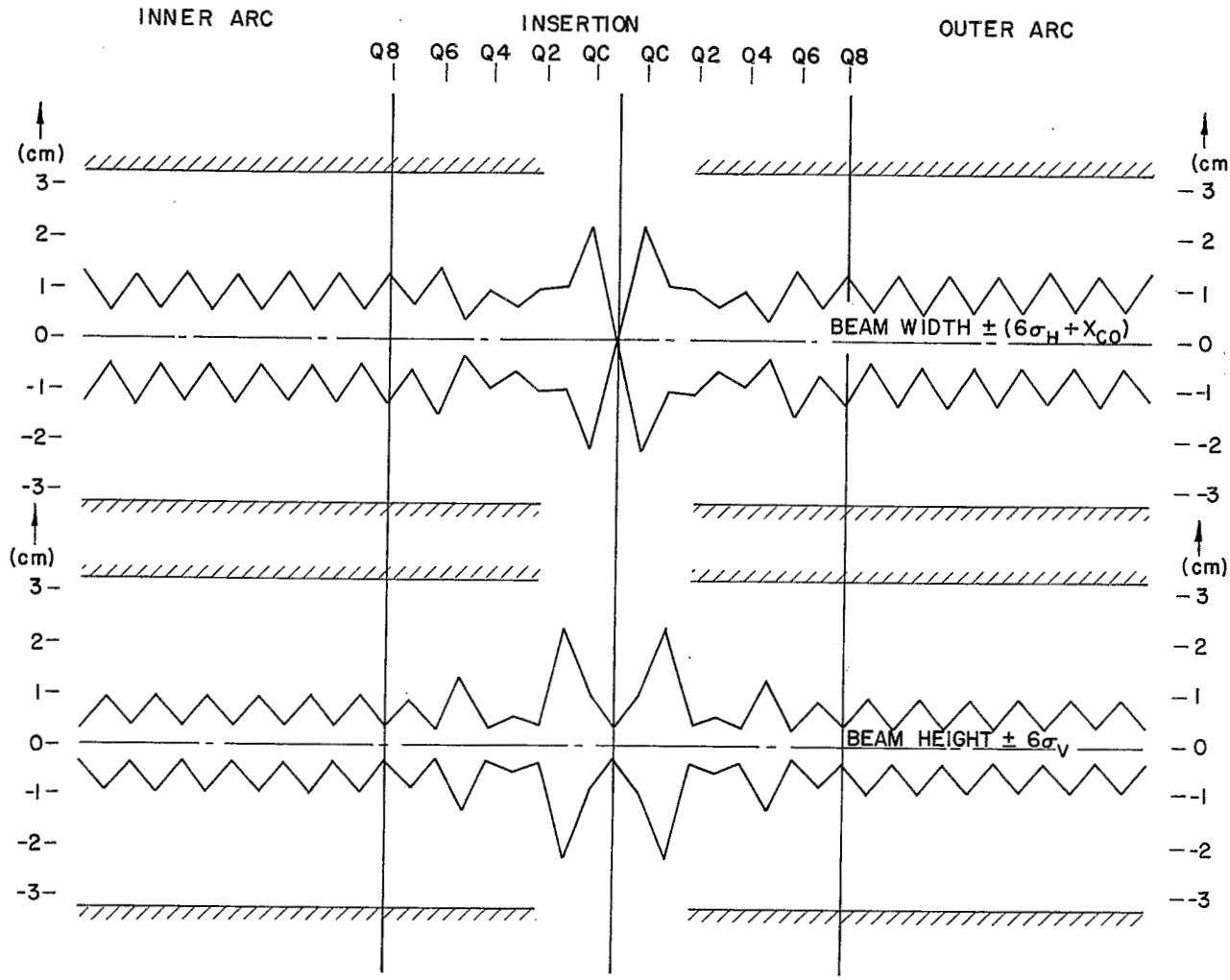

Fig. 26. Width and height of the Au beam after 10 hours at $\gamma = 100$ ($\varepsilon_N = 27.8 \times 10^{-6}$ π rad-m, $\Delta p/p \pm 2.7 \times 10^{-3}$)

region of ± 45 mm, if one wants to allow full performance over a period of 10 hours for $\gamma \geq 30$.

7. Chromatic Effects, Sextupoles, and Correction Elements

8. Vacuum Considerations

9. Beam-Beam Tune-Shift. Microwave Instability. Summary of the Dependence on the Ion Species

Beam-Beam Tune-Shift. The largest beam-beam tune-shift for a given number N_B of particles per bunch occurs for head-on collision. For a "round" beam, that is the emittances are the same in both planes and $\beta_V^* = \beta_H^*$, the tune-shift does not depend on the beam energy

$$\Delta\nu_o = \frac{3N_B r_o Z^2}{2\pi\varepsilon_N A} \tag{8}$$

where $r_o = 1.535 \times 10^{-18}$ m and ε_N is the normalized emittance for 95% of the beam in πm-rad units.

But for unequal β^*-values, the tune-shift is

$$\Delta\nu_{H,V} = \frac{2\Delta\nu_o}{1 + \sigma^*_{V,H}/\sigma^*_{H,V}} \tag{9}$$

where $\sigma^*_{H,V}$ are the rms beam dimensions at the crossing point. In the case in which the two beam have different ion species, the tune-shift on beam number "1" from beam number "2" is

$$\Delta\nu_{H,V(1)} = \frac{3N_2 r_o Z_1 Z_2}{2\pi\varepsilon_{N_2} A_1} \frac{2}{(1+\sigma^*_{V,H}/\sigma^*_{H,V})_2} . \tag{10}$$

Assuming an horizontal crossing, since $\beta_H^* < \beta_V^*$, the larger tuneshift occurs in the vertical plane. This is given in Table 17 for the case $\beta_H^* = 0.9$ m, $\beta_V^* = 6.3$ m and for colliding beams of the same species. The values shown are the initial ones, that is, for a normalized emittance of 10 πmm-mrad. With the exception of gold, all the numbers in Table 17 are larger than the canonically accepted value of 0.005. We show in the same Table N_{BB}, the number of acceptable particles per bunch. Nevertheless, with the exception of the proton beam, a slight increase of the original emittance as for instance caused by intrabeam scattering would easily reduce the other values below 0.005.

For crossing at an angle, the initial tune-shifts are smaller than those given by eqs. (8) and (9). Assuming an initial rms bunch length of 50 cm and a total crossing angle of 2 mrad, the tune-shift is always below 0.005 even assuming the number of particles per bunch as given in Table 7, excluding the proton beam.

Table 17. Beam-Beam Tune-Shift for Head-On Collision (Initial Values)

Element	$\Delta\nu_V$	N_{BB}
Proton	0.052	96×10^9
Deuterium	0.0052	96
Carbon	0.0068	16
Sulphur	0.0053	6.0
Copper	0.0062	3.6
Iodine	0.0060	2.2
Gold	0.0036	(1.53)

Microwave-Instability. The following limitation applies for the longitudinal coupling impedance in order to limit microwave instability within a bunch:

$$|Z/n| \lesssim 3 \frac{E|\eta|}{eI_p} \left(\frac{\sigma_E}{E}\right)^2 \frac{A}{Z^2}. \qquad (11)$$

On the right Z in the charge in units of the electron charge.

We have already seen the relevance of this relation at the transition energy where

$$\eta = \frac{1}{\gamma_T^2} - \frac{1}{\gamma^2}$$

vanishes. We now calculate this limit at the top energy where $|\eta| = 0.001435$. The peak current is given by eq. (6) with an initial rms bunch length of 50 cm, and the energy and the number of particles per bunch are given in Table 7. The results are shown in Table 18. The rms energy spread σ_E/E corresponds to an initial bunch area of 1.0 eV/A-sec. The worst case is for the proton beam.

Table 18. Longitudinal Coupling Impedance Limit

Element	E	I_p	σ_E/E	$\lvert Z/n \rvert$
Proton	252 GeV/A	47.8 Amp. part.	0.16×10^{-3}	0.6 ohm
Deuterium	126	4.8	0.32	23.
Carbon	126	1.1	0.32	17.
Sulfur	126	0.31	0.32	22.
Copper	116	0.215	0.34	20.
Iodine	105	0.124	0.38	24.
Gold	101	0.053	0.40	41.

Summary of the dependence on the Ion Species. Table 19 summarizes the information. Assuming the number N_B of particles per bunch that the source can deliver as shown in Table 7, we give the average electric current i_{ave}. There is less than a factor of two between iodine and gold which is very important for estimating beam loading of the rf system. Even for iodine the beam induced voltage is around 1 MV and this should be an acceptable situation. But there are clearly too many protons!

In Table 19 we have also listed the quantity $N_B\ (Z^2/A)$. This parameter is a measure of the beam-beam tune-shift and of the microwave instability (as well as of all other coherent and incoherent space charge effects). A133H0ç in this case there are too many protons per bunch. On the other hand all the other species from deuterium up to gold have about a comparable factor.

Last we list the quantity $N_B\ (Z^2/A)^2$ which is a measure of the intrabeam scattering. The effect is very strong for gold and iodine and is considerably less for lighter ions down to deuterium. For the proton beam case, because of the large number of particles available, the effect is strong again. A proton beam with 10^{12} particles per bunch causes high beam loading in the rf system; thus to estimate the luminosity performance we will assume 10^{11} protons per bunch.

10. Luminosity Performance

For head-on collisions the luminosity is given by

$$L_o = \frac{N_B^{\,2}\ B\ f_{rev}}{4\pi\sigma_H^* \sigma_V^*}. \qquad (12)$$

N_B is the number of particles per bunch, B the number of bunches per beam, f_{rev} the revolution frequency, and σ_H^*, σ_V^* are respectively the horizontal and verti-

Table 19. Bunch Intensity Scaling with Ion Species

Element	N_B x 10^9	$i_{electric}$ mA	$N_B \frac{Z^2}{A}$ x 10^9	$N_B (\frac{Z^2}{A})^2$ x 10^9
Proton	1000	750	1000	1000
Deuterium	100	75	50	25
Carbon	22	99	66	198
Sulphur	6.4	77	51	410
Copper	4.5	98	60	802
Iodine	2.6	103	57.5	1272
Gold	1.1	65	35	1104

cal rms beam dimensions at the crossing point. Eq. (12) applies to the case of two identical beams. For crossing at an angle (total) α, assuming the crossing is in the horizontal plane, the luminosity becomes

$$L = \frac{L_o}{\sqrt{1+p^2}} \quad \text{where } p = \frac{\alpha\sigma_\ell}{2\sigma^*_H} \tag{13}$$

and where σ_ℓ is the rms bunch length.

As we have seen, at the crossing point

$$\eta^* = 0 \text{ m}, \beta^*_H = 0.9 \text{ m} \quad \text{and} \quad \beta^*_V = 6.3 \text{ m}.$$

With these values we can estimate the initial luminosity, that is the luminosity at the beginning of the storage period, using the figures of Table 7. The results are given in Table 20 and they correspond to the top energy which for each

Table 20. Peak Luminosity ($cm^{-2}s^{-1}$) for Same Ion Species Colliding at Top Energy

	Crossing Angle, α (mrad)		
	0.0	2.0	
Proton ($N_B = 10^{11}$)	1.2	0.3	x 10^{31}
Deuterium	11.9	3.0	10^{30}
Carbon	5.8	1.4	10^{29}
Sulphur	4.9	1.2	10^{28}
Copper	22.6	5.0	10^{27}
Iodine	6.7	1.6	10^{27}
Gold	1.29	0.3	10^{27}

specie is as shown in Table 7, and to an initial rms bunch length of 0.5 m. As one can see the luminosity is reduced only by a factor of $\sqrt{4}$ for the large angle crossing.

At lower energies, down to 10 GeV/A, the luminosity will decrease linearly with γ for head-on collision and with $\sqrt{\gamma}$ for the large angle crossing. The dependence of the peak luminosity on energy is given in Fig. 27 for the special case of gold vs. gold.

Over a period of storage, because the beam dimensions are increasing from intrabeam scattering, the actual luminosity will decrease. The average luminosity normalized to the peak luminosity L_{ave}/L_o is plotted in Fig. 28 vs. beam energy (γ) for the case of gold on gold and head-on collision. For energies larger than 30 GeV/A the average luminosity over a period of 10 hours is about one-half of the peak luminosity. At 20 GeV/A it is 40% and at the injection energy ($\gamma = 12$) it is down to 50 for a running period of two hours. A similar behaviour, if not better, can be expected for the crossing angle cases.

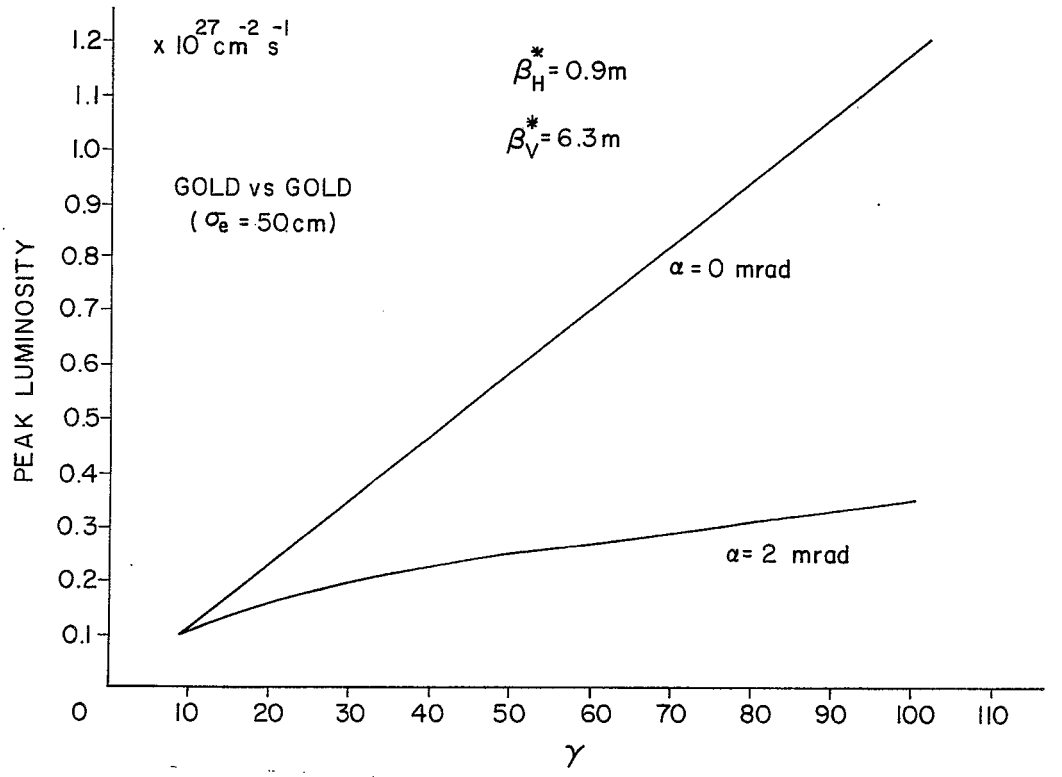

Fig. 27. Peak luminosity vs. energy (γ)

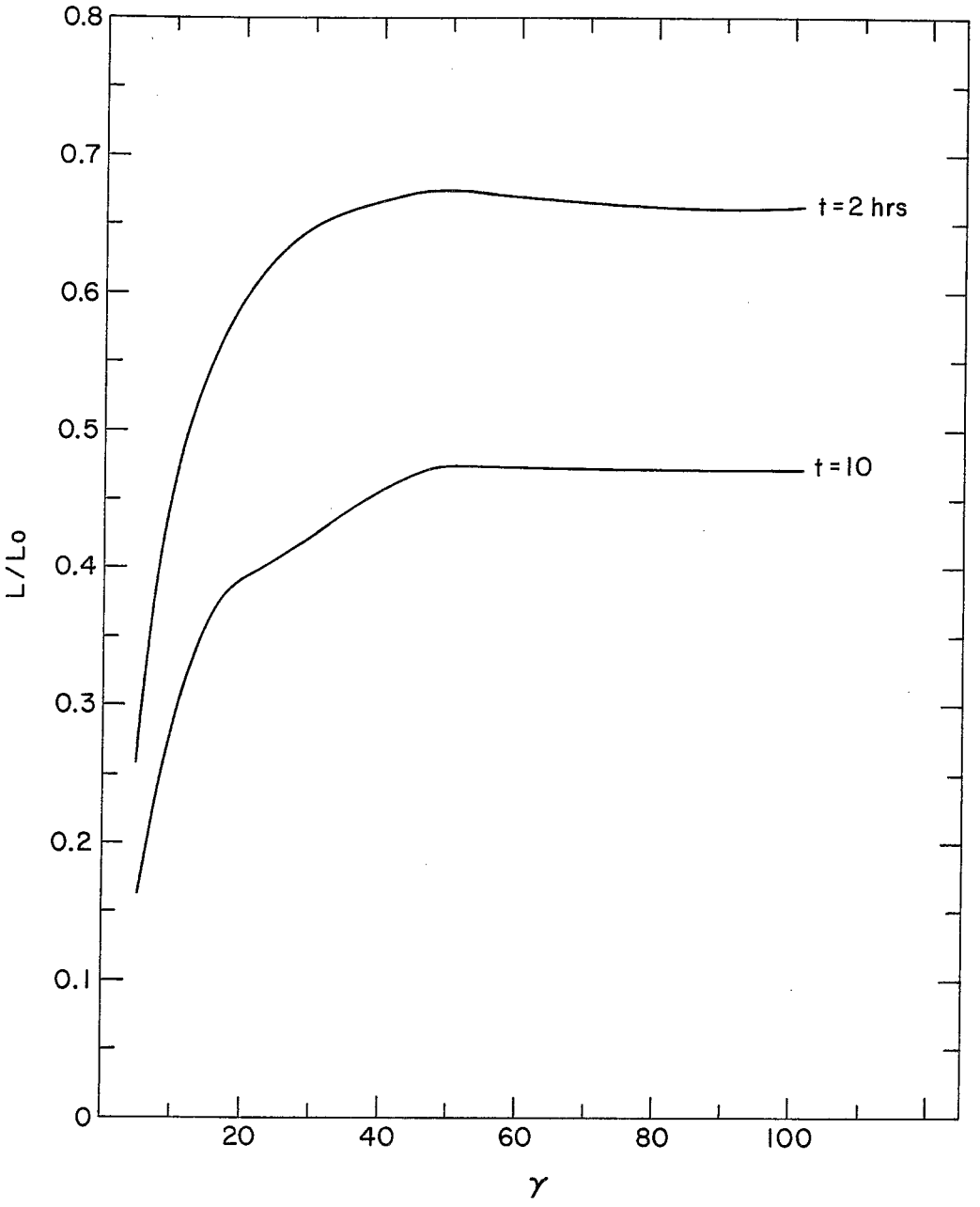

Fig. 28. Average luminosity normalized to its peak value vs. beam energy (γ)

Even at the low energy of 10 GeV/A the average luminosity can be well above 10^{25} $cm^{-2}sec^{-1}$ for gold on gold.

An important parameter required for the design of the detectors is the length σ_I of the interaction region. Its rms value is

$$\sigma_I = \frac{\sigma_\ell}{2+p} \tag{14}$$

where p is given by eq. (13). For head-on collision p = 0 and σ_I is half of the rms bunch length which is given in Fig. 19. For gold σ_I varies from 25 to 75 cm over a period of 10 hours at 100 GeV/A. It is about constant, around 25 - 35 cm at 30 GeV/A, but grows from 30 to 80 cm at the low energy end (10 GeV/A).

The interaction region is considerably shorter for crossing at an angle. For the top energy case the rms value is 10 cm for 2 mrad crossing angle. These values do not change significantly over a period of 10 hours and are about the same for all species involved.